

---

# Denoising Score Matching with Random Features: Insights on Diffusion Models from Precise Learning Curves

---

Anand Jerry George<sup>1</sup> Rodrigo Veiga<sup>1</sup> Nicolas Macris<sup>1</sup>

## Abstract

We derive asymptotically precise expressions for test and train errors of denoising score matching (DSM) in generative diffusion models. The score function is parameterized by random features neural networks, with the target distribution being  $d$ -dimensional standard Gaussian. We operate in a regime where the dimension  $d$ , number of data samples  $n$ , and number of features  $p$  tend to infinity while keeping the ratios  $\psi_n = \frac{n}{d}$  and  $\psi_p = \frac{p}{d}$  fixed. By characterizing the test and train errors, we identify regimes of generalization and memorization in diffusion models. Furthermore, our work sheds light on the conditions enhancing either generalization or memorization. Consistent with prior empirical observations, our findings indicate that the model complexity ( $p$ ) and the number of noise samples per data sample ( $m$ ) used during DSM significantly influence generalization and memorization behaviors.

## 1. Introduction

Generative models are at the heart of the on-going revolution in artificial intelligence. Formally, they aim to generate new samples from an unknown probability distribution, given  $n$  i.i.d. samples drawn from it. Commercial generative models demonstrate remarkable capabilities across various modalities, including text, speech, images, and videos, with new advancements being reported regularly. The impressive capabilities of these generative models are mainly driven by two key architectures: *transformers* and *diffusion models*. While transformers excel primarily on text data, diffusion models show exceptional proficiency in generating natural-looking images from text prompts. Despite their success, the scientific community remains divided on whether these models are truly creative or merely imitate based on the ex-

amples that they have seen during training (Ukpaka, 2024; Kamb & Ganguli, 2024). An even more pressing concern is that of *memorization*, where the model’s response partially or fully resembles training data. The memorization phenomenon raises serious implications, particularly regarding the privacy of data used to train these models (Carlini et al., 2021; 2023). The limited theoretical understanding of these models prevents addressing such questions effectively.

In this study, we focus on diffusion models and provide a detailed characterization of their learning task. It involves accurately estimating the *score* function associated with perturbed versions of the target distribution. Several studies have focused on analyzing the learning process in diffusion models (Chen et al., 2023b; Oko et al., 2023; Cui et al., 2023; 2025; Shah et al., 2023). These efforts have largely concentrated on the generalization properties of the learned score. However, a theoretical study of memorization aspects of diffusion models has been done only with the *empirical optimal score* function (Biroli et al., 2024; Achilli et al., 2024) (see Section 2.2). On the other hand, empirical results have demonstrated the occurrence of memorization when neural networks are employed, as is common in practice (Somepalli et al., 2023; 2024; Carlini et al., 2023; Zhang et al., 2024; Yoon et al., 2023; Gu et al., 2023; Ross et al., 2024). This gap in theory and practice raises an important question: can the phenomenon of memorization be theoretically shown when using a parametric class of functions for the score function? This is precisely the context of our study. By analyzing the learning process of a specific diffusion model instance, we provide insights into generalization and memorization in diffusion models.

### 1.1. Main Contributions

In this section, we provide a brief overview of the key contributions and findings of our work. Our study focuses on the learning aspect of diffusion models, which is to learn the score function of perturbed versions of a target distribution  $P_0$ , given in (2). The score function is obtained by minimizing a loss function called *denoising score matching* objective (see 5) over a parametric class of functions. The class of functions that we consider is the random features neural network, and the target distribution is the  $d$ -dimensional

---

<sup>1</sup>École Polytechnique Fédérale de Lausanne (EPFL), Lab for Statistical Mechanics of Inference in Large Systems (SMILS), CH-1015 Lausanne, Switzerland. Correspondence to: Anand Jerry George <anand.george@epfl.ch>.

standard Gaussian distribution. Let  $n$  denote the number of samples,  $d$  the data dimension and  $p$  the number of features of random feature neural network. We operate in a regime where  $d, n, p \rightarrow \infty$ , while the ratios  $\psi_n = \frac{n}{d}$  and  $\psi_p = \frac{p}{d}$  are kept fixed. The denoising score matching involves an additional parameter  $m$ , which is the number of noise samples per data sample used in forming the loss function, Eq. (5). In this setting, we make the following contributions:

- We analytically compute the test and train errors of the minimizer of denoising score matching loss.
- Using the obtained test and train errors, we study the generalization and memorization behavior in diffusion models.
- We show that a crossover transition between generalization and memorization behaviors occurs when the number of features equals the number of samples.
- We demonstrate that increasing the value of  $m$  enhances generalization when  $p < n$ , while it intensifies memorization when  $p > n$ .

Our observations and findings can be schematically summarized in the phase diagram presented in Fig. 1.

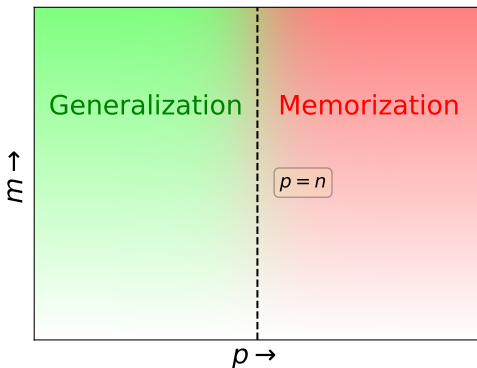


Figure 1. Phase diagram showing regimes of generalization and memorization. The gradient in color with  $m$  indicates the change in strength of the phenomenon.

We consider the simple isotropic Gaussian as the target distribution for two primary reasons. First, when studying the memorization phenomenon, the exact form of the distribution is less critical, as the focus lies on the specific samples used during training. Second, this choice provides an analytically tractable setting, allowing for a more precise theoretical analysis.

## 1.2. Related Works

**Diffusion models** Diffusion models (Sohl-Dickstein et al., 2015; Song & Ermon, 2019; Ho et al., 2020; Song et al.,

2020) rely on the non-equilibrium dynamics of a diffusion process for generative modeling. Since their introduction, there were several improvements (Dhariwal & Nichol, 2021; Rombach et al., 2022; Ho & Salimans, 2021; Nichol et al., 2022) that led them to become the state-of-the-art in generative modeling of images. Further, the design aspects of diffusion models was studied in (Karras et al., 2022).

## Sampling accuracy, generalization, and memorization

Several works have investigated the theoretical aspects of diffusion models. Sampling accuracy of the generative process in terms of distance from the target distribution was derived in (Chen et al., 2022; Benton et al., 2023; Chen et al., 2023a; Bortoli, 2022) for various settings. These works assume that the score function has been learned *a priori* with a certain level of accuracy. The score learning process was studied in (Cui et al., 2023; Shah et al., 2023; Han et al., 2023). The works (Kadkhodaie et al., 2023; Chen et al., 2023b; Wang et al., 2024) performed an end-to-end study of diffusion models giving a better understanding of their generalization properties. Further, the critical nature of feature emergence in diffusion models was studied in (Li & Chen, 2024; Sclocchi et al., 2025). More recently, statistical physics tools were employed to study the memorization phenomenon in the high-dimensional regime for models using the empirical optimal score function (Biroli et al., 2024; Raya & Ambrogioni, 2023; Ambrogioni, 2024; Achilli et al., 2024).

## 1.3. Our Techniques

In the setting briefly described in Section 1.1 and to be detailed in Section 3, we analytically compute the test and train errors of the minimizer of the denoising score matching loss. Our theoretical results are summarized in Theorem 3.2 and Theorem 3.5. Two main ingredients allowing the computation of exact asymptotic learning curves are the *Gaussian equivalence principle* (Gerace et al., 2020; Goldt et al., 2022; Hu & Lu, 2023) and the theory of *linear pencils* (Far et al., 2006; Helton et al., 2018; Adlam & Pennington, 2020; Bodin, 2024). We briefly describe them here.

**Gaussian Equivalence Principle** Suppose  $W \in \mathbb{R}^{p \times d}$ , and  $X \in \mathbb{R}^{d \times n}$  are random matrices with i.i.d. Gaussian entries. Let  $\varrho$  be a non-linear function and let  $F = \varrho\left(\frac{W}{\sqrt{d}}X\right)$ , where  $\varrho$  acts element-wise on a matrix. Then the Gaussian equivalence principle states that in the calculation of test and train errors, it is asymptotically equivalent to substitute  $F$  with the matrix  $\hat{F} = \mu_0 \mathbf{1}_p \mathbf{1}_n^T + \mu_1 \frac{W}{\sqrt{d}}X + v\Omega$ , where  $\Omega \in \mathbb{R}^{p \times n}$  is a random matrix with i.i.d. Gaussian entries, independent of  $W, X$ . The coefficients are given by  $\mu_0 = \mathbb{E}_g[\varrho(g)]$ ,  $\mu_1 = \mathbb{E}_g[\varrho(g)g]$ ,  $v^2 = \mathbb{E}_g[\varrho(g)^2] - \mu_0^2 - \mu_1^2$ , where  $g \sim \mathcal{N}(0, 1)$ .

**Linear Pencils** The theory of linear pencils is a powerful technique allowing to compute traces of rational functions involving random matrices with Gaussian entries. It amounts to constructing an appropriate block matrix called *linear pencil*, whose inverse gives the desired rational functions. For further details on the linear pencils method, we refer the reader to Chapter 3 of (Bodin, 2024).

In our context, the test and train errors can be expressed as a sum of traces of rational functions of random matrices. Some of these matrices have non-Gaussian entries due to the presence of an activation function  $\varrho$ . We circumvent this by using the Gaussian equivalence principle and, subsequently, the linear pencils method to compute the traces.

#### 1.4. Notations

We denote the  $d$ -dimensional Gaussian distribution with mean  $\mu$  and covariance  $\Sigma$  by  $\mathcal{N}(\mu, \Sigma)$ . The  $d$ -dimensional identity matrix is denoted by  $I_d$ , and  $\mathbf{1}_d$  denotes the  $d$ -dimensional all ones vector.  $\|\cdot\|$  denotes the  $l_2$  norm of a vector, while  $\|\cdot\|_F$  denotes the Frobenius norm of a matrix. The operator  $\nabla$  represents the gradient of a scalar function.

## 2. Preliminaries

### 2.1. Diffusion Models

Consider a set of  $n$  i.i.d. samples  $\mathcal{S} = \{x_1, x_2, \dots, x_n\}$  from an unknown distribution  $P_0$  on  $\mathbb{R}^d$ . Generative modeling aims to leverage the information in  $\mathcal{S}$  to draw new samples from  $P_0$ . Diffusion models address the problem by time reversing a diffusion process that transports  $P_0$  to a known distribution such as the isotropic Gaussian. In this work, we let the forward process to be an Ornstein-Uhlenbeck (OU) process (Gardiner, 2009) governed by the following stochastic differential equation (SDE):

$$dX_t = -X_t dt + \sqrt{2} dB_t, \quad X_0 \sim P_0. \quad (1)$$

Here,  $B_t$  is a standard  $d$ -dimensional Brownian motion. The distribution of  $X_t$  given  $X_0$  can be computed in closed form and is given by  $\mathcal{N}(a_t X_0, h_t I_d)$ , where  $a_t = e^{-t}$ , and  $h_t = 1 - e^{-2t}$  (hence,  $a_t^2 + h_t = 1$ ). As  $t \rightarrow \infty$ , the distribution of  $X_t$  converges to the  $d$ -dimensional standard Gaussian, regardless of  $X_0$ , since  $a_t \rightarrow 0$  and  $h_t \rightarrow 1$ .

Let  $P_t$  denote the probability distribution of  $X_t$ :

$$P_t(x) = (2\pi h_t)^{-d/2} \int_{\mathbb{R}^d} dP_0(x_0) e^{-\frac{\|x - a_t x_0\|^2}{2h_t}}. \quad (2)$$

Then, for a fixed  $T > 0$  and  $Y_T \sim P_T$ , we define the *time reversal* of the forward process (1) as

$$-dY_t = (Y_t + 2\nabla \log P_t(Y_t)) dt + \sqrt{2} d\tilde{B}_t, \quad (3)$$

where the SDE runs backward in time starting from  $Y_T$ , and  $\tilde{B}_t$  is a different instance of standard Brownian motion. The

term *time reversal* here means that the distributions of  $Y_t$  and  $X_t$  are identical for every  $t$  (Anderson, 1982; Haussmann & Pardoux, 1986). If we initiate the backward process with  $Y_T \sim P_T$ , the distribution of  $Y_0$  will be  $P_0$ . However, since  $P_T$  is unknown due to the lack of knowledge of  $P_0$ , we instead start the reverse process with  $Y_T \sim \mathcal{N}(0, I_d)$ . This approximation introduces minimal error, owing to the exponentially fast convergence of the OU process to  $\mathcal{N}(0, I_d)$ .

The main ingredient required to implement the backward process in (3) is  $\nabla \log P_t$ , known as the *score* function of  $P_t$ . In diffusion models, the learning task amounts to estimating the function  $\nabla \log P_t$  using the dataset  $\mathcal{S}$  of samples drawn from  $P_0$ . We consider minimizing the following score matching (Hyvärinen, 2005) objective for this:

$$\mathcal{L}_{\text{SM}}(s) = \int_0^T dt \mathbb{E}_{x_t \sim P_t} \left[ \|s(t, x_t) - \nabla \log P_t(x_t)\|^2 \right].$$

The above loss function is not practical, as  $\nabla \log P_t(x)$  is unknown. However, it is possible to construct an equivalent objective, the denoising score matching (DSM) loss (Vincent, 2011):

$$\mathcal{L}_{\text{DSM}}(s) = \int_0^T dt w(t) \mathbb{E} \|s(t, x_t) - \nabla \log P_t(x_t|x_0)\|^2,$$

where  $w$  is a weighting function and the expectation is with respect to  $x_0$  and  $x_t$ . In Appendix A.1 we show that  $\mathcal{L}_{\text{DSM}}$  is equal to  $\mathcal{L}_{\text{SM}}$  up to a time dependent scaling factor and offset. Hence, the minimizer of  $\mathcal{L}_{\text{DSM}}$  is same as the minimizer of  $\mathcal{L}_{\text{SM}}$ . Following (Song et al., 2020), we choose the weighting function to be  $w(t) = (\mathbb{E}_{x_0, x_t} \|\nabla \log P_t(x_t|x_0)\|^2)^{-1}$ . For OU process, we can compute  $\nabla \log P_t(x_t|x_0)$  in closed form. We can write  $x_t \sim P_t$  as  $x_t = a_t x_0 + \sqrt{h_t} z$ , where  $x_0 \sim P_0$ ,  $z \sim \mathcal{N}(0, I_d)$  are independent rvs and  $a_t = e^{-t}$ ,  $h_t = 1 - e^{-2t}$ . Consequently,  $\nabla \log P_t(x_t|x_0) = -\frac{(x_t - a_t x_0)}{h_t} = -\frac{z}{\sqrt{h_t}}$ . The weight function is given by  $w(t) = \frac{h_t}{d}$ . Substituting these, we can write the  $\mathcal{L}_{\text{DSM}}$  as

$$\mathcal{L}_{\text{DSM}}(s) = \int_0^T dt \frac{1}{d} \mathbb{E} \left\| \sqrt{h_t} s(t, a_t x_0 + \sqrt{h_t} z) + z \right\|^2,$$

where the expectation is with respect to  $x_0$  and  $z$ . Since  $P_0$  is unknown and only samples from it are available, we use an empirical estimate to approximate the expectation with respect to  $x_0$ . With  $y_i^t(z) = a_t x_i + \sqrt{h_t} z$ , we define

$$\mathcal{L}_{\text{DSM}}^\infty(s) = \int_0^T dt \frac{1}{dn} \sum_{i=1}^n \mathbb{E}_z \left\| \sqrt{h_t} s(t, y_i^t(z)) + z \right\|^2. \quad (4)$$

When  $s$  is a complicated function such as a neural network, it is difficult to compute even the expectation with respect to  $z$ . If we use an empirical estimate for the expectation with

respect to  $z$  as well, we get the following loss function,

$$\mathcal{L}_{\text{DSM}}^m(s) = \int_0^T dt \frac{1}{dnm} \sum_{i,j=1}^{n,m} \left\| \sqrt{h_t} s(t, y_{ij}^t) + z_{ij}^t \right\|^2 \quad (5)$$

where  $y_{ij}^t = a_t x_i + \sqrt{h_t} z_{ij}^t$ .

## 2.2. Empirical Optimal Score and Memorization

Consider the loss function given in (4). It has an unique minimizer:

$$s^e(t, x) = \nabla \log P_t^e(x), \quad (6)$$

where  $P_t^e$  is given by

$$P_t^e(x) = \frac{1}{n(2\pi h_t)^{d/2}} \sum_{i=1}^n e^{-\frac{\|x - a_t x_i\|^2}{2h_t}}. \quad (7)$$

The score  $s^e$  is often referred to as the *empirical optimal score*. A backward process using this score converges in distribution to the empirical distribution of the dataset  $\mathcal{S}$  as  $t \rightarrow 0$ . That is, the backward process collapses to one of the data samples as  $t \rightarrow 0$ . This is intimately connected to the memorization phenomenon in diffusion models as explored in (Biroli et al., 2024), although their study focuses on the regime where  $n = O(e^d)$ .

*Inspired by this connection, we define memorization as occurring when the score function learned using denoising score matching closely approximates the empirical optimal score function instead of the exact score.*

## 2.3. Random Features Model

In practice, the score function  $s$  is typically chosen from a parametric class of functions, and the DSM objective (5) is minimized within this class, with appropriate regularization. In this work, we represent the score function using a *random features* neural network (RFNN) (Rahimi & Recht, 2007). A RFNN is a two-layer neural network in which the first layer weights are randomly chosen and fixed, while the second layer weights are learned during training. It is a function from  $\mathbb{R}^d$  to  $\mathbb{R}^d$  of the form  $s_A(x|W) = \frac{A}{\sqrt{p}} \varrho\left(\frac{W}{\sqrt{d}}x\right)$ , where  $W \in \mathbb{R}^{p \times d}$  is a random matrix with its elements chosen i.i.d. from  $\mathcal{N}(0, 1)$ ,  $\varrho$  is an activation function acting element-wise and  $A \in \mathbb{R}^{d \times p}$  are the second layer weights that need to be learned. The RFNN is a simple neural network amenable to theoretical analysis and is able to capture interesting characteristics observed in more complicated neural network models, such as the double descent curve related to overparametrized regimes (Mei & Montanari, 2022; Bodin & Macris, 2021).

## 3. Main Results

We study the denoising score matching loss  $\mathcal{L}_{\text{DSM}}^m$  given in (5) when the score function is modeled using a RFNN and

$P_0 \equiv \mathcal{N}(0, I_d)$ . Our results characterize the asymptotic learning curves (test and train errors) of the minimizer of  $\mathcal{L}_{\text{DSM}}^m$  (5) in this setting. We analytically compute the learning curves for two extreme values of  $m$ :  $m = 1$  and  $m = \infty$ . These correspond to the extremes of the number of noise samples per data sample used during score learning. Based on the derived learning curves, we discuss the generalization and memorization behaviors in diffusion models.

We assume that at each time instant  $t$ , a different instance of RFNN is used to learn the score function specific to that time. Although this is a simplification compared to the methods employed in practice, it has been adopted in prior theoretical studies, e.g., (Cui et al., 2023). When using a different instance of RFNN at each  $t$ , note that minimizing the DSM loss (5) is equivalent to minimizing the integrand therein at each time instant. Henceforth, we focus on minimizing the DSM loss for a fixed time instant  $t$ . Introducing a regularization parameter  $\lambda > 0$ , the loss function becomes:

$$\begin{aligned} \mathcal{L}_t^m(A_t) = & \frac{1}{dnm} \sum_{i,j=1}^{n,m} \left\| \sqrt{h_t} \frac{A_t}{\sqrt{p}} \varrho\left(\frac{W_t}{\sqrt{d}} y_{ij}^t\right) + z_{ij}^t \right\|^2 \\ & + \frac{h_t \lambda}{dp} \|A_t\|_F^2, \end{aligned} \quad (8)$$

where we recall that  $y_{ij}^t = a_t x_i + \sqrt{h_t} z_{ij}^t$  with  $z_{ij}^t \sim \mathcal{N}(0, I_d)$ . We emphasize that  $W_t$  is a different and independent random matrix for each time  $t$ , and  $A_t$  is learned separately at each  $t$ . Denote  $\hat{A}_t$  as the second layer weights learned by some learning algorithm minimizing (8). The respective performance is evaluated by the test and train errors defined as follows:

$$\begin{aligned} \mathcal{E}_{\text{test}}^m(\hat{A}_t) = & \frac{1}{d} \mathbb{E}_{x \sim P_t} \left\| \frac{\hat{A}_t}{\sqrt{p}} \varrho\left(\frac{W_t}{\sqrt{d}} x\right) - \nabla \log P_t(x) \right\|^2, \\ \mathcal{E}_{\text{train}}^m(\hat{A}_t) = & \frac{1}{dnm} \sum_{i=1}^n \sum_{j=1}^m \left\| \sqrt{h_t} \frac{\hat{A}_t}{\sqrt{p}} \varrho\left(\frac{W_t}{\sqrt{d}} y_{ij}^t\right) + z_{ij}^t \right\|^2. \end{aligned}$$

The quantities  $\mathcal{E}_{\text{test}}^m$  and  $\mathcal{E}_{\text{train}}^m$  are random, where the randomness comes from  $W_t$ ,  $\{x_i\}_{i=1}^n$ , and  $\{z_{ij}^t\}_{i,j=1}^{n,m}$ . We expect them to concentrate on their expectations as  $d \rightarrow \infty$ .

The rationale behind studying the test and training errors of DSM to assess the performance of diffusion models stems from their direct connection to the model's generative accuracy. Specifically, as described in (Song et al., 2021), the error in diffusion models can be upper bounded using the test error. Suppose  $\hat{P}_t$  denotes the probability distribution of the backward process when we use the learned score function instead of the true score, and assume that  $\hat{P}_T = P_T$ . Then, the Kullback-Leibler (KL) divergence between  $P_0$  and  $\hat{P}_0$  can be upper bounded as  $D_{KL}(P_0 \parallel \hat{P}_0) \leq \frac{d}{2} \int_0^T dt \mathcal{E}_{\text{test}}^m(\hat{A}_t)$ .



### 3.1. Infinite Noise Samples per Data Sample: $m = \infty$

For  $m = \infty$ , the average over  $z_{ij}^t$  in the DSM loss becomes an expectation. Letting  $y_i^t(z) = a_t x_i + \sqrt{h_t} z$ , we write

$$\mathcal{L}_t^\infty(A_t) = \frac{1}{dn} \sum_{i=1}^n \mathbb{E}_z \left\| \sqrt{h_t} \frac{A_t}{\sqrt{p}} \varrho \left( \frac{W_t}{\sqrt{d}} y_i^t(z) \right) + z \right\|^2 + \frac{h_t \lambda}{dp} \|A_t\|_F^2. \quad (9)$$

We characterize the minimizer of the above loss function in the asymptotic regime where  $d, n, p \rightarrow \infty$ , while keeping the ratios  $\psi_n = \frac{n}{d}$  and  $\psi_p = \frac{p}{d}$  fixed. We make the following assumption about the the activation function  $\varrho$ .

**Assumption 3.1.** The activation function  $\varrho$  has a Hermite polynomial expansion given by  $\varrho(y) = \sum_{l=0}^{\infty} \mu_l \text{He}_l(y)$ , where  $\text{He}_l$  is the  $l^{\text{th}}$  Hermite polynomial. For ease of presentation, assume that  $\mu_0 = 0$ . The  $L_2$  norm of  $\varrho$  with respect to standard Gaussian measure is denoted by  $\|\varrho\|$ , with  $P^\gamma$  denoting the bivariate standard Gaussian distribution with correlation coefficient  $\gamma$  (see Eq. (12) in the Appendix B). The function  $c$  is defined as  $c(\gamma) = \mathbb{E}_{u,v \sim P^\gamma} [\varrho(u)\varrho(v)]$ .

With these notations and assumptions, the following theorem characterizes the test and train errors of the denoising score matching loss for  $m = \infty$  case.

**Theorem 3.2.** Suppose  $P_0 \equiv \mathcal{N}(0, I_d)$  and  $\varrho$  satisfies Assumption 3.1. Let  $s^2 = \|\varrho\|^2 - c(a_t^2) - h_t \mu_1^2$ ,  $v_0^2 = c(a_t^2) - a_t^2 \mu_1^2$ , and  $v^2 = \|\varrho\|^2 - \mu_1^2$ . Let  $\psi_n = \frac{n}{d}$ , and  $\psi_p = \frac{p}{d}$ . Let  $\zeta_1, \zeta_2, \zeta_3, \zeta_4$  be the solution of the following set of algebraic equations as a function of  $q$  and  $z$ .

$$\begin{aligned} \zeta_1(s^2 - z + a_t^2 \mu_1^2 \zeta_2 \zeta_4 + v_0^2 \zeta_2 + (h_t \mu_1^2 + q) \zeta_4) - 1 &= 0, \\ \zeta_2(\psi_n + v_0^2 \psi_p \zeta_1 - a_t \mu_1 \zeta_3) - \psi_n &= 0, \\ a_t \mu_1 \psi_p \zeta_1(1 + a_t \mu_1 \zeta_2 \zeta_3) + (1 + (h_t \mu_1^2 + q) \psi_p \zeta_1) \zeta_3 &= 0, \\ a_t^2 \mu_1^2 \psi_p \zeta_1 \zeta_2 \zeta_4 + (1 + (h_t \mu_1^2 + q) \psi_p \zeta_1) \zeta_4 - 1 &= 0. \end{aligned}$$

Define the function  $\mathcal{K}(q, z) = -\frac{\zeta_3(q, z)}{a_t \mu_1}$ . Let  $e_1 = \mathcal{K}(0, -\lambda)$ ,  $e_2 = -\frac{\partial \mathcal{K}}{\partial q}(0, -\lambda)$ ,  $e_3 = \frac{\partial \mathcal{K}}{\partial z}(0, -\lambda)$ . Then, for the minimizer of (9)  $\hat{A}_t$ , as  $d, n, p \rightarrow \infty$ :

$$\begin{aligned} \lim_{d, n, p \rightarrow \infty} \mathbb{E} \left[ \mathcal{E}_{\text{test}}^\infty(\hat{A}_t) \right] &= 1 - 2\mu_1^2 e_1 + \mu_1^4 e_2 + \mu_1^2 v^2 e_3, \\ \lim_{d, n, p \rightarrow \infty} \mathbb{E} \left[ \mathcal{E}_{\text{train}}^\infty(\hat{A}_t) \right] &= 1 - h_t \mu_1^2 e_1 - \lambda h_t \mu_1^2 e_3. \end{aligned}$$

We defer the proof to Appendix B.

**Remark 3.3.** We expect  $\mathcal{E}_{\text{test}}^\infty(\hat{A}_t)$  and  $\mathcal{E}_{\text{train}}^\infty(\hat{A}_t)$  to concentrate on their expectations as  $d \rightarrow \infty$ . However, a rigorous proof of this result is beyond the scope of the current work. Henceforth, we use the term test (train) error for both  $\mathcal{E}_{\text{test}}^\infty$  ( $\mathcal{E}_{\text{train}}^\infty$ ) and  $\mathbb{E}[\mathcal{E}_{\text{test}}^\infty]$  ( $\mathbb{E}[\mathcal{E}_{\text{train}}^\infty]$ ), interchangeably.

Theorem 3.2 can be used to compute the test and train errors for different values of  $t, \psi_n, \psi_p$ .

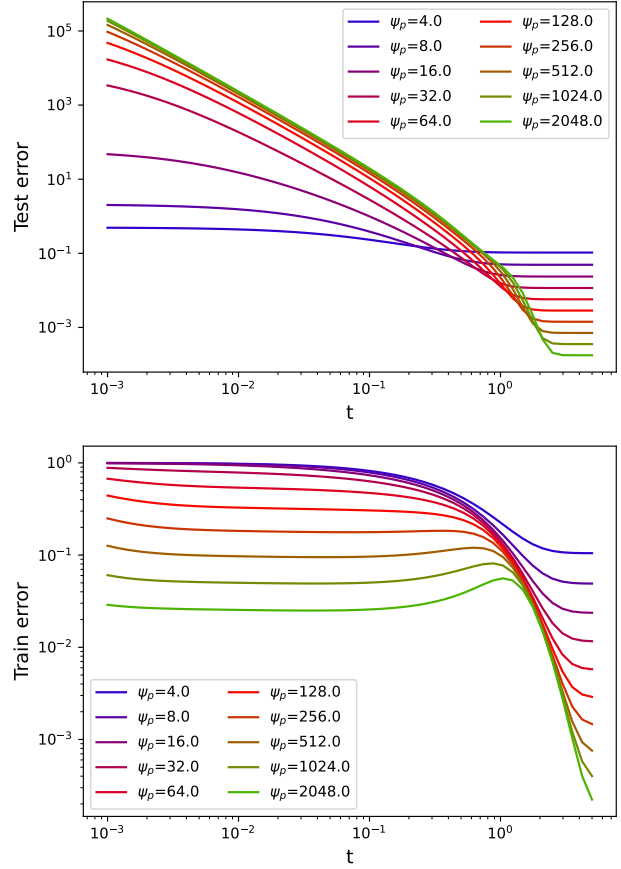


Figure 2. Learning curves for  $m = \infty$ , with  $\psi_n = 20.0$ ,  $\lambda = 0.001$ . The activation function is ReLU.

Fig. 2 shows the learning curves as a function of  $t$  for different values of  $\psi_p$  and a fixed  $\psi_n$ . We can comprehend them by decomposing  $\mathcal{E}_{\text{train}}^\infty(\hat{A}_t)$  into bias and variance components through the following Lemma.

**Lemma 3.4.** Suppose  $\mathcal{M}_t$  and  $\mathcal{V}_t$  are given by

$$\begin{aligned} \mathcal{M}_t &= \frac{1}{dn} \sum_{i=1}^n \mathbb{E}_z \left\| \frac{\hat{A}_t}{\sqrt{p}} \varrho \left( \frac{W_t}{\sqrt{d}} y_i(t, z) \right) - s^e(t, y_i^t(z)) \right\|^2, \\ \mathcal{V}_t &= \frac{1}{dn} \sum_{i=1}^n \mathbb{E}_z \left\| \sqrt{h_t} s^e(t, y_i^t(z)) + z \right\|^2, \end{aligned}$$

where  $s^e$  is the empirical optimal score function given in (6). Then,  $\mathcal{E}_{\text{train}}^\infty(\hat{A}_t) = \mathcal{V}_t + h_t \mathcal{M}_t$ .

Lemma 3.4 is proved in Appendix A.2.

We discuss the behavior of  $\mathcal{M}_t$  and  $\mathcal{V}_t$  for different values of  $t$ , thereby explaining the learning curves in Fig. 2. The parameter  $\psi_p$  is used to control the approximation power

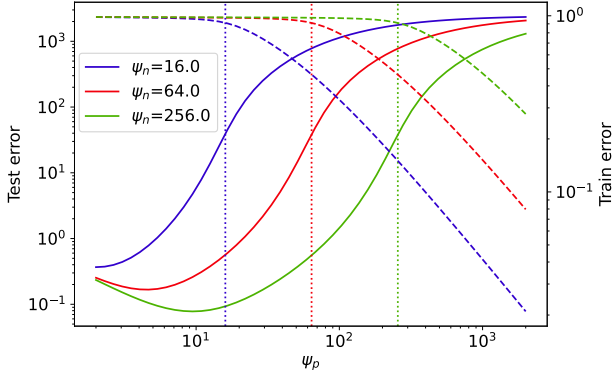


Figure 3. Learning curves for  $m = \infty$ , with  $t = 0.01$ ,  $\lambda = 0.001$ ,  $\varrho \equiv \text{ReLU}$ . The solid lines are for test error and dashed lines are for train error. The dotted vertical lines are for  $\psi_p = \psi_n$ .

of RFNNs. A general observation is that, since  $\mathcal{V}_t$  is independent of  $\hat{A}_t$ , any change in  $\mathcal{E}_{\text{train}}^\infty(\hat{A}_t)$  as  $\psi_p$  varies must be attributed to the changes in  $\mathcal{M}_t$ . A smaller value of  $\mathcal{M}_t$  indicates that the learned score function is closer to the empirical optimal score function, as its definition suggests. A score function close to the empirical optimal score function can negatively affect the generalization performance of diffusion models. This can be understood as follows: For small  $t$ ,  $h_t \approx 0$ , and hence, in the neighborhood of  $a_t x_i$ ,  $P_t^e$  is dominated by the  $i^{\text{th}}$  term in the summation (7). Therefore, in the vicinity of  $a_t x_i$ , we have  $s^e(t, x) \approx -\frac{x - a_t x_i}{h_t}$ . In the backward process, this translates to a component in the drift that points towards  $a_t x_i$ . Consequently, the trajectories will tend to move toward training samples, causing the output of the backward process to resemble one of the training samples. This behavior is referred to as *memorization*, which occurs when the learned score function closely approximates the empirical optimal score function. With this understanding, we now qualitatively discuss the learning curves in Fig. 2 for different values of  $t$ .

- $t = \infty$ : At  $t = \infty$ , we have  $a_t = 0$ ,  $h_t = 1$  and  $s^e(t, y) = -y$ . Substituting these, we get  $\mathcal{E}_{\text{train}}^\infty(\hat{A}_t) = \mathcal{M}_t = \mathbb{E}_z \left\| \frac{\hat{A}_t}{\sqrt{p}} \varrho \left( \frac{W_t}{\sqrt{d}} z \right) + z \right\|^2$ . Hence, the train and test errors are equal, and depends only on how well the RFNN can approximate a linear function. As  $\psi_p$  increases, the approximation power of the RFNN increases, and thus the train and test errors decrease.
- $t \gg 1$ : In this regime, we still have  $s^e(t, y) \approx -y$ , giving  $\mathcal{V}_t \approx a_t^2$ . Hence,  $\mathcal{E}_{\text{train}}^\infty(\hat{A}_t) \approx h_t \mathcal{M}_t + a_t^2$ . When  $\psi_p$  is large,  $\mathcal{M}_t$  is small, and the train error is dominated by the  $a_t^2$  term. Therefore, we see that train error increases rapidly as  $t$  decreases. However, the test error remains constant, since it is approximately equal to  $\mathcal{M}_t$ .

- $t \ll 1$ : At these times, the empirical optimal score function satisfies  $s^e(t, a_t x_i + \sqrt{h_t} z) \approx -\frac{z}{\sqrt{h_t}}$  for any data point  $x_i$ . Consequently,  $\mathcal{V}_t \approx 0$ . This leads to the result  $\mathcal{E}_{\text{train}}^\infty(\hat{A}_t) \approx h_t \mathcal{M}_t$ . In this regime, the train error depends on how well RFNN can approximate the empirical optimal score function  $s^e$ . With an increase in  $\psi_p$ , the approximation power increases and the train error decreases. However, since the actual score function significantly deviates from the empirical score function in this regime, the test error increases rapidly with  $\psi_p$ . In the neighborhood of  $a_t x_i$ , learning the empirical optimal score function instead of the actual score makes the drift in the backward process to pull the trajectories towards  $a_t x_i$ . Thus, if the backward trajectory comes in the vicinity of  $a_t x_i$  at time  $t$ , the diffusion model tend to recover the sample  $x_i$ .

The analysis of Fig. 2 hints that the RFNN starts to show memorization behavior for  $t < 1$  and large values of  $\psi_p$ . To explore this further, we plot in Fig. 3 the learning curves as a function of  $\psi_p$  for different values of  $\psi_n$  and keeping  $t$  fixed and small. From the plot, we observe the following: 1) For  $\psi_p \ll \psi_n$ , the train error remains constant and test error is small, indicating generalization. 2) For  $\psi_p \gg \psi_n$ , the train error is small and test error is high indicating the presence of memorization. 3) In the region  $\psi_p \approx \psi_n$ , the test error rises rapidly, signaling the onset of memorization.

Thus,  $\psi_p = \psi_n$  acts as a crossover point at which the behavior of the score transitions from generalization phase to memorization phase. This transition is depicted in Fig. 1 as a phase diagram. We note that this shift in behavior is not a sharp transition but rather a gradual change.

More figures illustrating the effects of  $\lambda$  and the activation function  $\varrho$  on test and train errors can be found in Appendices D.2 and D.3.

### 3.2. Single Noise Sample per Data Sample: $m = 1$

For  $m = 1$ , the DSM loss (8) reduces to

$$\mathcal{L}^1(A_t) = \frac{1}{dn} \sum_{i=1}^n \left\| \sqrt{h_t} \frac{A_t}{\sqrt{p}} \varrho \left( \frac{W_t}{\sqrt{d}} y_i^t \right) + z_i^t \right\|^2 + \frac{h_t \lambda}{dp} \|A_t\|_F^2. \quad (10)$$

The following theorem characterizes the test and train errors of minimizer of the loss given in (10).

**Theorem 3.5.** *Let  $P_0 \equiv \mathcal{N}(0, I_d)$ , and  $\varrho$  satisfies Assumption 3.1. Let  $v^2 = \|\varrho\|^2 - \mu_1^2$ ,  $\psi_n = \frac{n}{d}$ , and  $\psi_p = \frac{p}{d}$ . Let  $\zeta_1, \zeta_2, \zeta_3, \zeta_4, \zeta_5$  be the solution of the following set of*

algebraic equations as a function of  $q$  and  $z$ .

$$\begin{aligned}\zeta_1(-z + q\zeta_2 + v^2\zeta_4 + \mu_1^2\zeta_2\zeta_4) - 1 &= 0, \\ \zeta_2(1 + q\psi_p\zeta_1) + \mu_1^2\psi_p\zeta_1\zeta_2\zeta_4 - 1 &= 0, \\ \zeta_3(1 + q\psi_p\zeta_1) + \mu_1\psi_p\zeta_1(1 + \mu_1\zeta_3\zeta_4) &= 0, \\ \zeta_4(\psi_n + v^2\psi_p\zeta_1 - \mu_1\zeta_3) - \psi_n &= 0, \\ \zeta_4(-h_t\mu_1\zeta_3\zeta_4 - 1) + \psi_n\zeta_5 &= 0.\end{aligned}$$

Define the function  $\mathcal{K}(q, z) = 1 - \psi_n\zeta_5(q, z)$ . Let  $e_1 = -\sqrt{h_t}\zeta_3(0, -\lambda)\zeta_4(0, -\lambda)$ ,  $e_2 = -\frac{\partial\mathcal{K}}{\partial q}(0, -\lambda)$ , and  $e_3 = \frac{\partial\mathcal{K}}{\partial z}(0, -\lambda)$ . Then, for the minimizer of (10)  $\hat{A}_t$ , as  $d, n, p \rightarrow \infty$ :

$$\begin{aligned}\lim_{d, n, p \rightarrow \infty} \mathbb{E} \left[ \mathcal{E}_{test}^1(\hat{A}_t) \right] &= 1 - \frac{2\mu_1}{\sqrt{h_t}}e_1 + \frac{\mu_1^2}{h_t}e_2 + \frac{v^2}{h_t}e_3, \\ \lim_{d, n, p \rightarrow \infty} \mathbb{E} \left[ \mathcal{E}_{train}^1(\hat{A}_t) \right] &= 1 - \mathcal{K}(0, -\lambda) - \lambda e_3.\end{aligned}$$

The proof is presented in Appendix C. Using the Theorem 3.5, we calculate the test and train errors as a function of  $t$ ,  $\psi_n$  and  $\psi_p$ , which is illustrated in Fig. 6 in Appendix D.1.

Fig. 6a shows the learning curves as a function of  $t$  for different values of  $\psi_p$  while keeping  $\psi_n$  fixed. The learning curves reveal several notable trends. The test error increases as  $t$  decreases; however, it shows a non-monotonic behavior with  $\psi_p$ . The train error decreases monotonically with increasing  $\psi_p$  for all  $t$ , indicating the model’s progressive capacity to interpolate the training data.

Note that for small  $t$ , the test error remains at least two orders of magnitude smaller than in the  $m = \infty$  case. Further, the test error decreases as  $\psi_p$  increases beyond  $\psi_n$ . These observations suggest that the model does not display memorization behavior when  $m$  equals 1. This contrasts the  $m = \infty$  case, where memorization significantly impacts the test error. These findings indicate that larger values of  $m$  increase the propensity of diffusion models to memorize the initial dataset, justifying the illustration in Fig. 1.

The DSM loss (10) shares similarities with the loss function used for RFNN in regression settings. Several works such as (Mei & Montanari, 2022; Bodin & Macris, 2021; Hu et al., 2024), have analyzed the learning curves of RFNN in regression contexts. Notably, they predict the presence of a double descent phenomenon, where the test error exhibits a peak at  $\psi_p = \psi_n$ , followed by a decrease for  $\psi_p < \psi_n$  or  $\psi_p > \psi_n$ . The point  $\psi_p = \psi_n$  is called interpolation threshold. In our study, we also observe the double descent phenomenon in the DSM setting with  $m = 1$ . This is depicted in Fig. 6b.

## 4. Numerical Experiments

In this section, we validate the analytical predictions made in the previous section through simulations. In addition, we

simulate the learning curves for intermediate values of  $m$ . Lastly, we present numerical results indicating memorization when the learned score function is used in the backward diffusion.

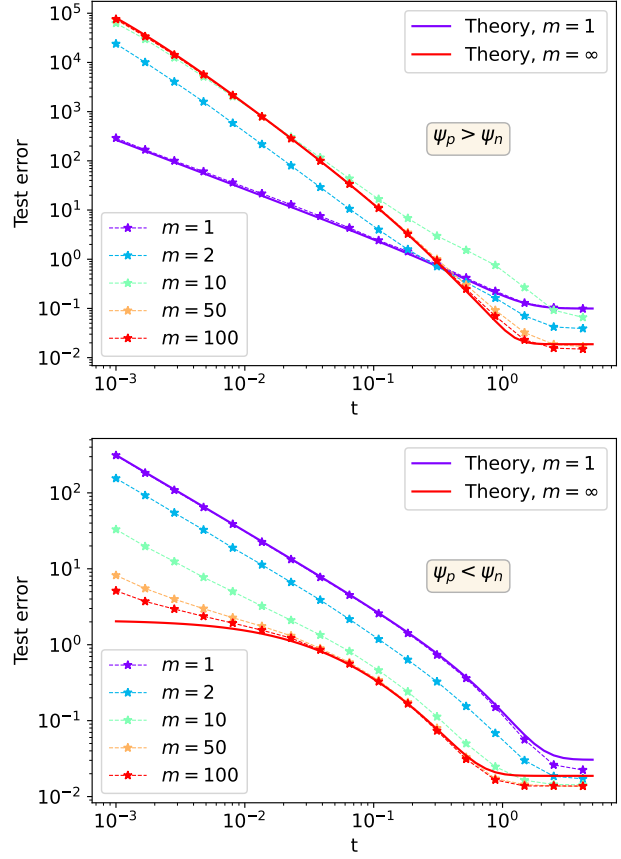


Figure 4. Simulation results ( $d = 100$ ) for different values of  $m$  and fixed  $\psi_p = 20$ ; with  $\psi_n = 2$  (upper plot) and  $\psi_n = 50$  (lower plot). Theoretical results for  $m = 1, \infty$  are depicted as solid lines.

Fig. 4 presents the test errors obtained numerically for various values of  $m$  (corresponding train errors can be found in Fig. 11 in Appendix E). The upper plot displays the learning errors for the case  $\psi_p > \psi_n$ , while the lower plot corresponds to  $\psi_p < \psi_n$ . Based on the previous discussions, memorization is expected when  $\psi_p > \psi_n$ , and this behavior is evident in Fig. 4 when  $t$  is small. Additionally, the extent of memorization increases with  $m$ , indicating that large  $m$  is detrimental to generalization (small test error) in this regime. This is in contrast to the behavior of test and train errors in the  $\psi_p < \psi_n$  regime, where the generalization improves as  $m$  increases, evidenced by a decrease in the test error.

The solid lines in Fig. 4 plots the analytical predictions derived in the previous section for  $m = 1$  and  $m = \infty$ . These predictions align closely with the numerical results for  $m = 1$  and  $m = 100$  respectively, validating its consis-

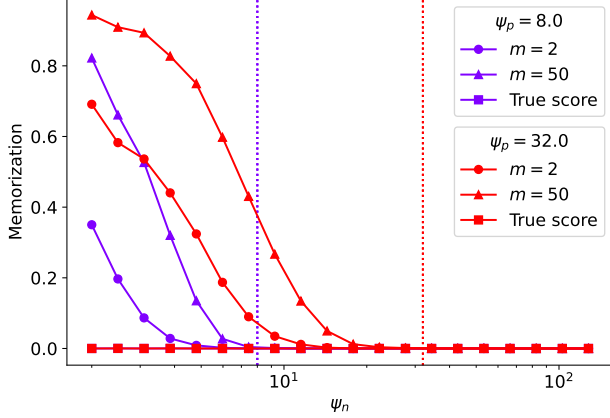


Figure 5. Results of experiment on memorization. We use  $N = 5000$  and  $\delta = 1/3$ . The dotted vertical lines are for  $\psi_n = \psi_p$ .

tency with the observed data. Minor mismatches between theoretical and numerical curves in the small  $t$  and large  $t$  regimes can be attributed to finite size effects.

Next, through experiments, we show the effect of memorization when the score function learned using RFNN is used in the backward diffusion. We demonstrate that, in the memorization regime, once the backward diffusion process enters the vicinity of a data sample, it exhibits a tendency to remain within that neighborhood. Specifically, we simulate  $N$  instances of the backward diffusion

$$-dY_t = \left( Y_t + 2s_{\hat{A}_t}(Y_t|W_t) \right) dt + \sqrt{2} d\tilde{B}_t,$$

where  $s_{\hat{A}_t}(y|W_t) = \frac{\hat{A}_t}{\sqrt{p}} \varrho\left(\frac{W_t}{\sqrt{d}}y\right)$  with  $\hat{A}_t$  being the minimizer of (8). We start the backward diffusion at time  $t_1 = 0.1$  in the vicinity of one of the training samples  $x_l$ . More precisely, we start the backward diffusion at  $Y_{t_1} = a_{t_1}x_l + \sqrt{h_{t_1}}z$ , where  $l$  is selected uniformly at random from the set  $\{1, 2, \dots, n\}$ , and  $z \sim \mathcal{N}(0, I_d)$ . We stop the simulation at  $t_0 = 10^{-5}$  and check whether  $Y_{t_0}$  is closer to one of the training samples compared to others (Yoon et al., 2023). In particular, let  $\text{NN}_i(x)$  denote the  $i^{\text{th}}$  nearest neighbor of  $x$  in  $\{x_1, x_2, \dots, x_n\}$ . We say that the backward diffusion retrieves a data sample if  $\frac{\|Y_{t_0} - \text{NN}_1(Y_{t_0})\|}{\|Y_{t_0} - \text{NN}_2(Y_{t_0})\|} < \delta$ , with  $\delta > 0$ . We measure memorization as the fraction of  $N$  backward diffusion instances that retrieves one of the data samples. Fig. 5 shows the measure of memorization thus obtained as a function of  $\psi_n$  for different values of  $\psi_p$  and  $m$ . We observe that the result of this experiment is in line with the predictions made in the previous sections. In particular, we note the following: 1) For  $m = 50$  and  $\psi_n < \psi_p$ , the memorization is high. 2) The memorization decreases as  $m$  decreases. 3) Memorization is zero when  $\psi_n > \psi_p$ .

## 5. Discussion and Future Work

In this work, we provided theoretical insights into the mechanisms underlying generalization and memorization in diffusion models. We studied generalization and memorization by analyzing the test and train errors of denoising score matching (DSM) with random features and unstructured data. To the best of our knowledge, this work is the first to provide a theoretical study of memorization when a parametric score is used. Memorization is typically observed in practice when the diffusion models are trained long enough using highly over parameterized neural networks. In line with these empirical observations, our findings indicate that the complexity of the model ( $p$ ) and the number of noise samples per data sample ( $m$ ) used during DSM play a significant role in memorization. In practical implementations,  $m$  increases as the number of training epochs increases.

As the complexity of the model increases, it can approximate more complex functions, leading to a better approximation of the empirical optimal score. Furthermore, as  $m$  increases, an optimizer of DSM loss (5) tends to be close to the empirical optimal score. These effects that lead to memorization are captured in our results and are illustrated as a phase diagram in Fig. 1. As expected, generalization occurs when the complexity of the model is limited, i.e.,  $p < n$ .

Our theoretical analysis was facilitated by several simplifications, which can also be viewed as limitations of this work. First, we employ RFNNs to represent the score function and study the minimizer of the corresponding DSM loss. This is a significant departure from practical implementations, where complex neural architectures are employed to parameterize the score function and gradient-based optimization methods are applied to find the minimizer. Furthermore, practical score parameterizations typically incorporate time  $t$  as an explicit argument, whereas we assume a separate instance of RFNN for each  $t$ , optimized independently. Lastly, our analysis focuses on unstructured data, while real-world datasets often possess various forms of structure.

Our work represents a preliminary step in understanding generalization and memorization in diffusion models. Future directions could focus on addressing some of the simplifications inherent in our analysis. Specifically, can we use a time-parameterized model for the score and derive its learning errors? Another direction is to analyze the entire backward diffusion using the learned score and demonstrate the generalization and memorization behaviors. These advancements could further improve our understanding on diffusion models.

## Acknowledgements

The work of A. J. G and R. V has been supported by Swiss National Science Foundation grant number 200021-204119.



## References

- Achilli, B., Ventura, E., Silvestri, G., Pham, B., Raya, G., Krotov, D., Lucibello, C., and Ambrogioni, L. Losing dimensions: Geometric memorization in generative diffusion, October 2024. arXiv:2410.08727.
- Adlam, B. and Pennington, J. The Neural Tangent Kernel in High Dimensions: Triple Descent and a Multi-Scale Theory of Generalization. In *Proceedings of the 37th International Conference on Machine Learning*, pp. 74–84. PMLR, November 2020. ISSN: 2640-3498.
- Ambrogioni, L. In Search of Dispersed Memories: Generative Diffusion Models Are Associative Memory Networks. *Entropy*, 26(5):381, April 2024. ISSN 1099-4300. doi: 10.3390/e26050381.
- Anderson, B. D. O. Reverse-time diffusion equation models. *Stochastic Processes and their Applications*, 12(3):313–326, May 1982.
- Benton, J., Bortoli, V. D., Doucet, A., and Deligiannidis, G. Nearly d-Linear Convergence Bounds for Diffusion Models via Stochastic Localization. In *The Twelfth International Conference on Learning Representations*, October 2023.
- Biroli, G., Bonnaire, T., de Bortoli, V., and Mézard, M. Dynamical regimes of diffusion models. *Nature Communications*, 15(1):9957, November 2024. ISSN 2041-1723. doi: 10.1038/s41467-024-54281-3. Publisher: Nature Publishing Group.
- Bodin, A. and Macris, N. Model, sample, and epoch-wise descents: exact solution of gradient flow in the random feature model. In *Advances in Neural Information Processing Systems*, volume 34, pp. 21605–21617. Curran Associates, Inc., 2021.
- Bodin, A. P. M. *Random matrix methods for high-dimensional machine learning models*. PhD thesis, EPFL, 2024.
- Bortoli, V. D. Convergence of denoising diffusion models under the manifold hypothesis. *Transactions on Machine Learning Research*, August 2022. ISSN 2835-8856.
- Carlini, N., Tramèr, F., Wallace, E., Jagielski, M., Herbert-Voss, A., Lee, K., Roberts, A., Brown, T., Song, D., Erlingsson, U., Oprea, A., and Raffel, C. Extracting Training Data from Large Language Models. In *30th USENIX Security Symposium (USENIX Security 21)*, pp. 2633–2650, 2021. ISBN 978-1-939133-24-3.
- Carlini, N., Hayes, J., Nasr, M., Jagielski, M., Sehwag, V., Tramèr, F., Balle, B., Ippolito, D., and Wallace, E. Extracting training data from diffusion models. In *Proceedings of the 32nd USENIX Conference on Security Symposium, SEC '23*, pp. 5253–5270, USA, August 2023. USENIX Association. ISBN 978-1-939133-37-3.
- Chen, H., Lee, H., and Lu, J. Improved analysis of score-based generative modeling: user-friendly bounds under minimal smoothness assumptions. In *Proceedings of the 40th International Conference on Machine Learning*, volume 202 of *ICML '23*, pp. 4735–4763, Honolulu, Hawaii, USA, July 2023a. JMLR.org.
- Chen, M., Huang, K., Zhao, T., and Wang, M. Score Approximation, Estimation and Distribution Recovery of Diffusion Models on Low-Dimensional Data. In *Proceedings of the 40th International Conference on Machine Learning*, pp. 4672–4712. PMLR, July 2023b. ISSN: 2640-3498.
- Chen, S., Chewi, S., Li, J., Li, Y., Salim, A., and Zhang, A. Sampling is as easy as learning the score: theory for diffusion models with minimal data assumptions. In *The Eleventh International Conference on Learning Representations*, September 2022.
- Cui, H., Krzakala, F., Vanden-Eijnden, E., and Zdeborova, L. Analysis of Learning a Flow-based Generative Model from Limited Sample Complexity. In *The Twelfth International Conference on Learning Representations*, October 2023.
- Cui, H., Pehlevan, C., and Lu, Y. M. A precise asymptotic analysis of learning diffusion models: theory and insights, January 2025. arXiv:2501.03937 [cs].
- Dhariwal, P. and Nichol, A. Diffusion Models Beat GANs on Image Synthesis. In *Advances in Neural Information Processing Systems*, volume 34, pp. 8780–8794. Curran Associates, Inc., 2021.
- Far, R. R., Oraby, T., Bryc, W., and Speicher, R. Spectra of large block matrices, October 2006. arXiv:cs/0610045.
- Gardiner, C. W. *Stochastic methods: a handbook for the natural and social sciences*. Number 13 in Springer series in synergetics. Springer, Berlin Heidelberg, 4th ed edition, 2009. ISBN 978-3-642-08962-6.
- Gerace, F., Loureiro, B., Krzakala, F., Mezard, M., and Zdeborova, L. Generalisation error in learning with random features and the hidden manifold model. In *Proceedings of the 37th International Conference on Machine Learning*, pp. 3452–3462. PMLR, November 2020. ISSN: 2640-3498.
- Goldt, S., Loureiro, B., Reeves, G., Krzakala, F., Mezard, M., and Zdeborova, L. The Gaussian equivalence of generative models for learning with shallow neural networks. In *Proceedings of the 2nd Mathematical and*

- Scientific Machine Learning Conference*, pp. 426–471. PMLR, April 2022. ISSN: 2640-3498.
- Gu, X., Du, C., Pang, T., Li, C., Lin, M., and Wang, Y. On Memorization in Diffusion Models, October 2023. arXiv:2310.02664 [cs].
- Han, Y., Razaviyayn, M., and Xu, R. Neural Network-Based Score Estimation in Diffusion Models: Optimization and Generalization. In *The Twelfth International Conference on Learning Representations*, October 2023.
- Hausmann, U. G. and Pardoux, E. Time Reversal of Diffusions. *The Annals of Probability*, 14(4):1188–1205, October 1986. Publisher: Institute of Mathematical Statistics.
- Helton, J. W., Mai, T., and Speicher, R. Applications of realizations (aka linearizations) to free probability. *Journal of Functional Analysis*, 274(1):1–79, January 2018.
- Ho, J. and Salimans, T. Classifier-Free Diffusion Guidance. In *NeurIPS 2021 Workshop on Deep Generative Models and Downstream Applications*, December 2021.
- Ho, J., Jain, A., and Abbeel, P. Denoising Diffusion Probabilistic Models. In *Advances in Neural Information Processing Systems*, volume 33, pp. 6840–6851. Curran Associates, Inc., 2020.
- Hu, H. and Lu, Y. M. Universality Laws for High-Dimensional Learning With Random Features. *IEEE Transactions on Information Theory*, 69(3):1932–1964, March 2023. Conference Name: IEEE Transactions on Information Theory.
- Hu, H., Lu, Y. M., and Misiakiewicz, T. Asymptotics of Random Feature Regression Beyond the Linear Scaling Regime, March 2024. arXiv:2403.08160.
- Hyvärinen, A. Estimation of Non-Normalized Statistical Models by Score Matching. *Journal of Machine Learning Research*, 6(24):695–709, 2005. ISSN 1533-7928.
- Kadkhodaie, Z., Guth, F., Simoncelli, E. P., and Mallat, S. Generalization in diffusion models arises from geometry-adaptive harmonic representations. In *The Twelfth International Conference on Learning Representations*, October 2023.
- Kamb, M. and Ganguli, S. An analytic theory of creativity in convolutional diffusion models, December 2024. arXiv:2412.20292 [cs].
- Karras, T., Aittala, M., Aila, T., and Laine, S. Elucidating the Design Space of Diffusion-Based Generative Models. *Advances in Neural Information Processing Systems*, 35: 26565–26577, December 2022.
- Kibble, W. F. An extension of a theorem of Mehler’s on Hermite polynomials. *Mathematical Proceedings of the Cambridge Philosophical Society*, 41(1):12–15, June 1945. ISSN 0305-0041, 1469-8064. doi: 10.1017/S0305004100022313.
- Li, M. and Chen, S. Critical windows: non-asymptotic theory for feature emergence in diffusion models. In *Proceedings of the 41st International Conference on Machine Learning*, pp. 27474–27498. PMLR, July 2024. ISSN: 2640-3498.
- Mei, S. and Montanari, A. The Generalization Error of Random Features Regression: Precise Asymptotics and the Double Descent Curve. *Communications on Pure and Applied Mathematics*, 75(4):667–766, 2022. eprint: <https://onlinelibrary.wiley.com/doi/pdf/10.1002/cpa.22008>.
- Nichol, A. Q., Dhariwal, P., Ramesh, A., Shyam, P., Mishkin, P., Mcgrew, B., Sutskever, I., and Chen, M. GLIDE: Towards Photorealistic Image Generation and Editing with Text-Guided Diffusion Models. In *Proceedings of the 39th International Conference on Machine Learning*, pp. 16784–16804. PMLR, June 2022. ISSN: 2640-3498.
- Oko, K., Akiyama, S., and Suzuki, T. Diffusion Models are Minimax Optimal Distribution Estimators. In *Proceedings of the 40th International Conference on Machine Learning*, pp. 26517–26582. PMLR, July 2023. ISSN: 2640-3498.
- Rahimi, A. and Recht, B. Random Features for Large-Scale Kernel Machines. In *Advances in Neural Information Processing Systems*, volume 20. Curran Associates, Inc., 2007.
- Raya, G. and Ambrogioni, L. Spontaneous symmetry breaking in generative diffusion models. In *Advances in Neural Information Processing Systems*, volume 36, pp. 66377–66389. Curran Associates, Inc., 2023.
- Rombach, R., Blattmann, A., Lorenz, D., Esser, P., and Ommer, B. High-Resolution Image Synthesis with Latent Diffusion Models. In *2022 IEEE/CVF Conference on Computer Vision and Pattern Recognition (CVPR)*, pp. 10674–10685, New Orleans, LA, USA, June 2022. IEEE.
- Ross, B. L., Kamkari, H., Wu, T., Hosseinzadeh, R., Liu, Z., Stein, G., Cresswell, J. C., and Loaiza-Ganem, G. A Geometric Framework for Understanding Memorization in Generative Models, October 2024. arXiv:2411.00113 [stat].
- Sclocchi, A., Favero, A., and Wyart, M. A phase transition in diffusion models reveals the hierarchical nature of data. *Proceedings of the National Academy of Sciences*, 122

- (1):e2408799121, January 2025. ISSN 0027-8424, 1091-6490. doi: 10.1073/pnas.2408799121.
- Shah, K., Chen, S., and Klivans, A. Learning Mixtures of Gaussians Using the DDPM Objective. *Advances in Neural Information Processing Systems*, 36:19636–19649, December 2023.
- Sohl-Dickstein, J., Weiss, E., Maheswaranathan, N., and Ganguli, S. Deep Unsupervised Learning using Nonequilibrium Thermodynamics. In *Proceedings of the 32nd International Conference on Machine Learning*, pp. 2256–2265. PMLR, June 2015. ISSN: 1938-7228.
- Somepalli, G., Singla, V., Goldblum, M., Geiping, J., and Goldstein, T. Diffusion Art or Digital Forgery? Investigating Data Replication in Diffusion Models. In *2023 IEEE/CVF Conference on Computer Vision and Pattern Recognition (CVPR)*, pp. 6048–6058, June 2023. ISSN: 2575-7075.
- Somepalli, G., Singla, V., Goldblum, M., Geiping, J., and Goldstein, T. Understanding and mitigating copying in diffusion models. In *Proceedings of the 37th International Conference on Neural Information Processing Systems, NIPS '23*, pp. 47783–47803, Red Hook, NY, USA, May 2024. Curran Associates Inc.
- Song, Y. and Ermon, S. Generative Modeling by Estimating Gradients of the Data Distribution. In *Advances in Neural Information Processing Systems*, volume 32. Curran Associates, Inc., 2019.
- Song, Y., Sohl-Dickstein, J., Kingma, D. P., Kumar, A., Ermon, S., and Poole, B. Score-Based Generative Modeling through Stochastic Differential Equations. In *International Conference on Learning Representations*, October 2020.
- Song, Y., Durkan, C., Murray, I., and Ermon, S. Maximum Likelihood Training of Score-Based Diffusion Models. In *Advances in Neural Information Processing Systems*, volume 34, pp. 1415–1428. Curran Associates, Inc., 2021.
- Ukpaka, P. M. The creative agency of large language models: a philosophical inquiry. *AI and Ethics*, September 2024. ISSN 2730-5953, 2730-5961. doi: 10.1007/s43681-024-00557-9.
- Vincent, P. A Connection Between Score Matching and Denoising Autoencoders. *Neural Computation*, 23(7): 1661–1674, July 2011. ISSN 0899-7667, 1530-888X. doi: 10.1162/NECO\_a\_00142.
- Wang, Y., He, Y., and Tao, M. Evaluating the design space of diffusion-based generative models. In *The Thirty-eighth Annual Conference on Neural Information Processing Systems*, November 2024.
- Yoon, T., Choi, J. Y., Kwon, S., and Ryu, E. K. Diffusion Probabilistic Models Generalize when They Fail to Memorize. In *ICML 2023 Workshop on Structured Probabilistic Inference and Generative Modeling*, July 2023.
- Zhang, H., Zhou, J., Lu, Y., Guo, M., Wang, P., Shen, L., and Qu, Q. The Emergence of Reproducibility and Consistency in Diffusion Models. In *Proceedings of the 41st International Conference on Machine Learning*, pp. 60558–60590. PMLR, July 2024. ISSN: 2640-3498.

## A. Score matching

### A.1. Proof that minimizers of $\mathcal{L}_{\text{DSM}}$ and $\mathcal{L}_{\text{SM}}$ are the same

From the  $L_2$  minimization property of conditional expectation, the minimizer of  $\mathcal{L}_{\text{DSM}}$  is given by  $\hat{s}(t, x) = \mathbb{E}[\nabla \log P_t(x_t|x_0) | x_t = x]$ . We have

$$\begin{aligned} \mathbb{E}[\nabla \log P_t(x_t|x_0) | x_t = x] &= \int dx_0 \frac{\nabla P_t(x_t = x|x_0)}{P_t(x_t = x|x_0)} P_t(x_0|x_t = x) \\ &= \int dx_0 \nabla P_t(x_t = x|x_0) \frac{P_0(x_0)}{P_t(x)} \\ &= \frac{1}{P_t(x)} \nabla \int dx_0 P_t(x_t = x|x_0) P_0(x_0) \\ &= \nabla \log P_t(x). \end{aligned}$$

Hence, we have shown that the minimizer of  $\mathcal{L}_{\text{DSM}}$  is same as the minimizer of  $\mathcal{L}_{\text{SM}}$ .

### A.2. Proof of Lemma 3.4

Let  $P_t^e$  denote the joint probability distribution of  $(y_t, z)$ , where  $y_t = a_t x + \sqrt{h_t} z$ ,  $x \sim \frac{1}{n} \sum_{i=1}^n \delta_{x_i}$  and  $z \sim \mathcal{N}(0, I_d)$ . We have

$$\begin{aligned} \mathcal{E}_{\text{train}}^\infty(\hat{A}_t) &= \frac{1}{dn} \sum_{i=1}^n \mathbb{E}_z \left\| \sqrt{h_t} \frac{\hat{A}_t}{\sqrt{p}} \varrho \left( \frac{W_t}{\sqrt{d}} (a_t x_i + \sqrt{h_t} z) \right) + z \right\|^2 \\ &= \frac{1}{d} \mathbb{E}_{P_t^e} \left[ \left\| \sqrt{h_t} \frac{\hat{A}_t}{\sqrt{p}} \varrho \left( \frac{W_t}{\sqrt{d}} y_t \right) + z \right\|^2 \right] \\ &\stackrel{(a)}{=} \frac{1}{d} \mathbb{E}_{P_t^e} \left[ \left\| \sqrt{h_t} \frac{\hat{A}_t}{\sqrt{p}} \varrho \left( \frac{W_t}{\sqrt{d}} y_t \right) - \sqrt{h_t} s^e(t, y_t) \right\|^2 + \left\| \sqrt{h_t} s^e(t, y_t) + z \right\|^2 \right] \\ &= h_t \mathcal{M}_t + \mathcal{V}_t. \end{aligned}$$

The equality (a) follows from the following:

$$\begin{aligned} &\mathbb{E}_{P_t^e} \left[ \left\langle \frac{\hat{A}_t}{\sqrt{p}} \varrho \left( \frac{W_t}{\sqrt{d}} y \right) - s^e(t, y), \sqrt{h_t} s^e(t, y) + z \right\rangle \right] \\ &= \mathbb{E}_{P_t^e} \left[ \mathbb{E} \left[ \left\langle \frac{\hat{A}_t}{\sqrt{p}} \varrho \left( \frac{W_t}{\sqrt{d}} y \right) - s^e(t, y), \sqrt{h_t} s^e(t, y) + z \right\rangle \middle| y \right] \right] \\ &= \mathbb{E}_{P_t^e} \left[ \left\langle \frac{\hat{A}_t}{\sqrt{p}} \varrho \left( \frac{W_t}{\sqrt{d}} y \right) - s^e(t, y), \sqrt{h_t} s^e(t, y) + \mathbb{E}[z | y] \right\rangle \right] \\ &= \mathbb{E}_{P_t^e} \left[ \left\langle \frac{\hat{A}_t}{\sqrt{p}} \varrho \left( \frac{W_t}{\sqrt{d}} y \right) - s^e(t, y), \sqrt{h_t} s^e(t, y) - \sqrt{h_t} \nabla \log P_t^e(y) \right\rangle \right] \\ &= 0, \end{aligned}$$

since we have  $\mathbb{E}[z | y] = -\sqrt{h_t} \nabla \log P_t^e(y)$ .



## B. Proof of Theorem 3.2

When  $m = \infty$ , the denoising score matching loss is given by

$$\begin{aligned} \mathcal{L}_t^\infty(A_t) &= \frac{1}{dn} \sum_{i=1}^n \mathbb{E}_z \left[ \left\| \sqrt{h_t} \frac{A_t}{\sqrt{p}} \varrho \left( \frac{W_t}{\sqrt{p}} (a_t x_i + \sqrt{h_t} z) \right) + z \right\|^2 \right] + \frac{h_t \lambda}{dp} \|A_t\|_F^2 \\ &= \frac{h_t}{d} \operatorname{tr} \left\{ \frac{A_t^T}{\sqrt{p}} \frac{A_t}{\sqrt{p}} U \right\} + \frac{2\sqrt{h_t}}{d} \operatorname{tr} \left\{ \frac{A_t}{\sqrt{p}} V \right\} + 1 + \frac{h_t \lambda}{d} \operatorname{tr} \left\{ \frac{A_t^T}{\sqrt{p}} \frac{A_t}{\sqrt{p}} \right\}, \end{aligned}$$

where

$$U = \frac{1}{n} \sum_{i=1}^n \mathbb{E}_z \left[ \varrho \left( \frac{W_t}{\sqrt{d}} (a_t x_i + \sqrt{h_t} z) \right) \varrho \left( \frac{W_t}{\sqrt{d}} (a_t x_i + \sqrt{h_t} z) \right)^T \right],$$

and

$$V = \frac{1}{n} \sum_{i=1}^n \mathbb{E}_z \left[ \varrho \left( \frac{W_t}{\sqrt{d}} (a_t x_i + \sqrt{h_t} z) \right) z^T \right].$$

Thus we get the optimal  $A_t$  as

$$\frac{\hat{A}_t}{\sqrt{p}} = -\frac{1}{\sqrt{h_t}} V^T (U + \lambda I_p)^{-1}. \quad (11)$$

Now, we compute test error (generalization error) and train error when  $P_0 \equiv \mathcal{N}(0, I_d)$ . We note that in this case,  $P_t$  remains  $\mathcal{N}(0, 1)$  for all  $t$ .

**Test Error:**

$$\begin{aligned} \mathcal{E}_{\text{test}}^\infty(\hat{A}_t) &= \frac{1}{d} \mathbb{E}_{x \sim P_t} \left[ \left\| \frac{\hat{A}_t}{\sqrt{p}} \varrho \left( \frac{W_t}{\sqrt{d}} x \right) - \nabla \log P_t(x) \right\|^2 \right] \\ &= \frac{1}{d} \mathbb{E}_{x \sim P_t} \left[ \left\| \frac{\hat{A}_t}{\sqrt{p}} \varrho \left( \frac{W_t}{\sqrt{d}} x \right) + x \right\|^2 \right] \\ &= 1 - \frac{2}{d} \operatorname{tr} \left\{ \frac{1}{\sqrt{h_t}} V^T (U + \lambda I_p)^{-1} \underbrace{\mathbb{E}_x \left[ \varrho \left( \frac{W_t}{\sqrt{d}} x \right) x^T \right]}_{:= \tilde{V}} \right\} \\ &\quad + \frac{1}{d} \operatorname{tr} \left\{ \frac{1}{h_t} (U + \lambda I_p)^{-1} V V^T (U + \lambda I_p)^{-1} \underbrace{\mathbb{E}_x \left[ \varrho \left( \frac{W_t}{\sqrt{d}} x \right) \varrho \left( \frac{W_t}{\sqrt{d}} x \right)^T \right]}_{:= \tilde{U}} \right\}. \end{aligned}$$

Since we focus on a single time instant, we drop the subscript  $t$  in the above expressions. However, it is important to note that  $a$  and  $h$  depend on  $t$ , and we have the relation  $a^2 + h = 1$ .

We need to compute  $V, U, \tilde{V}, \tilde{U}$  in order to get an expression for  $\mathcal{E}_{\text{test}}^\infty$ . We will first consider  $\tilde{V}$ :

$$\tilde{V} = \mathbb{E}_x \left[ \varrho \left( \frac{W}{\sqrt{d}} x \right) x^T \right].$$

Let  $P^\gamma$  denote the bivariate standard Gaussian distribution with correlation coefficient  $\gamma$ . Explicitly,

$$P^\gamma(x, y) = \frac{1}{2\pi\sqrt{1-\gamma^2}} e^{-\frac{x^2+y^2-2\gamma xy}{2(1-\gamma^2)}}. \quad (12)$$

Let  $w_i$  denote the  $i^{\text{th}}$  row of  $W$ . For large  $d$ ,  $\frac{\|w_i\|^2}{d}$  concentrates to 1. Then:

$$\begin{aligned}\tilde{V}_{ij} &= \mathbb{E}_x \left[ \varrho \left( \frac{w_i^T x}{\sqrt{d}} \right) x_j \right] \\ &= \mathbb{E}_{(u,v) \sim P \frac{w_{ij}}{\sqrt{d}}} [\varrho(u) v] \\ &\stackrel{(a)}{=} \sum_{k=0}^{\infty} \frac{\left(\frac{w_{ij}}{\sqrt{d}}\right)^k}{k!} \mathbb{E}_u [\varrho(u) \mathbf{He}_k(u)] \mathbb{E}_v [v \mathbf{He}_k(v)] \\ &= \mu_1 \frac{w_{ij}}{\sqrt{d}},\end{aligned}$$

where in (a) we used the Mehler Kernel formula (Kibble, 1945). Hence, we have  $\tilde{V} = \mu_1 \frac{W}{\sqrt{d}}$ . Now, we consider  $\tilde{U}$ :

$$\begin{aligned}\tilde{U}_{ij} &= \mathbb{E}_x \left[ \varrho \left( \frac{w_i^T x}{\sqrt{d}} \right) \varrho \left( \frac{w_j^T x}{\sqrt{d}} \right) \right] \\ &= \mathbb{E}_{(u,v) \sim P \frac{w_i^T w_j}{d}} [\varrho(u) \varrho(v)] \\ &= \sum_{k=0}^{\infty} \frac{\left(\frac{w_i^T w_j}{d}\right)^k}{k!} \mathbb{E}_u [\varrho(u) \mathbf{He}_k(u)] \mathbb{E}_v [\varrho(v) \mathbf{He}_k(v)] \\ &= \sum_{k=0}^{\infty} \frac{\left(\frac{w_i^T w_j}{d}\right)^k}{k!} \mathbb{E}_u [\varrho(u) \mathbf{He}_k(u)]^2.\end{aligned}$$

Let  $\mu_0 = \mathbb{E}_g[\varrho(g)]$ ,  $\mu_1 = \mathbb{E}_g[\varrho(g)g]$ ,  $\|\varrho\|^2 = \mathbb{E}_g[\varrho(g)^2]$ , where  $g \sim \mathcal{N}(0, 1)$ . Then, we have

$$\tilde{U}_{ij} = \begin{cases} \mu_0^2 + \mu_1^2 \frac{w_i^T w_j}{d} + O(1/d) & \text{if } i \neq j, \\ \|\varrho\|^2 & \text{if } i = j. \end{cases}$$

Let  $v^2 = \|\varrho\|^2 - \mu_0^2 - \mu_1^2$ . The  $O(1/d)$  term cannot give rise to a  $O(1)$  change in the asymptotic spectrum. Hence, we neglect it. We have

$$\tilde{U} = \mu_0^2 \mathbf{1}_p \mathbf{1}_p^T + \mu_1^2 \frac{W W^T}{\sqrt{d} \sqrt{d}} + v^2 I_p.$$

Now we will consider  $V$ . Let

$$V^l = \mathbb{E}_z \left[ \varrho \left( \frac{W}{\sqrt{d}} (ax_l + \sqrt{h}z) \right) z^T \right].$$

We have

$$\begin{aligned}V_{ij}^l &= \mathbb{E}_z \left[ \varrho \left( \frac{w_i^T (ax_l + \sqrt{h}z)}{\sqrt{d}} \right) z_j \right] \\ &= \mathbb{E}_{(u,v) \sim P \frac{w_{ij}}{\sqrt{d}}} \left[ \varrho \left( \frac{aw_i^T x_l}{\sqrt{d}} + \sqrt{h}u \right) v \right] \\ &= \sum_{k=0}^{\infty} \frac{\left(\frac{w_{ij}}{\sqrt{d}}\right)^k}{k!} \mathbb{E}_u \left[ \varrho \left( \frac{aw_i^T x_l}{\sqrt{d}} + \sqrt{h}u \right) \mathbf{He}_k(u) \right] \mathbb{E}_v [v \mathbf{He}_k(v)] \\ &= \frac{w_{ij}}{\sqrt{d}} \mathbb{E}_u \left[ \varrho \left( \frac{aw_i^T x_l}{\sqrt{d}} + \sqrt{h}u \right) u \right] \\ &= \frac{w_{ij}}{\sqrt{d}} \varrho_1 \left( \frac{aw_i^T x_l}{\sqrt{d}} \right),\end{aligned}$$

where  $\varrho_1(y) = \mathbb{E}_u [\varrho(y + \sqrt{h}u)]$ . Summing over the  $n$  data samples:

$$\begin{aligned}
 V_{ij} &= \frac{1}{n} \sum_{l=1}^n V_{ij}^l \\
 &= \frac{w_{ij}}{\sqrt{d}} \frac{1}{n} \sum_{l=1}^n \varrho_1 \left( \frac{aw_i^T x_l}{\sqrt{d}} \right) \\
 &= \frac{w_{ij}}{\sqrt{d}} \mathbb{E}_x \left[ \varrho_1 \left( \frac{aw_i^T x}{\sqrt{d}} \right) \right] + O(1/d) \\
 &= \frac{w_{ij}}{\sqrt{d}} \mathbb{E}_g [\varrho_1(ag)] + O(1/d) \\
 &= \frac{w_{ij}}{\sqrt{d}} \mathbb{E}_{g,u} [\varrho(ag + \sqrt{h}u)] + O(1/d) \\
 &= \sqrt{h}\mu_1 \frac{w_{ij}}{\sqrt{d}} + O(1/d).
 \end{aligned}$$

Neglecting  $O(1/d)$  terms, we have  $V = \sqrt{h}\mu_1 \frac{W}{\sqrt{d}}$ . Now, let's consider  $U$ . Let

$$U^l = \mathbb{E}_z \left[ \varrho \left( \frac{W}{\sqrt{d}}(ax_l + \sqrt{h}z) \right) \varrho \left( \frac{W}{\sqrt{d}}(ax_l + \sqrt{h}z) \right)^T \right].$$

For  $i \neq j$  we have,

$$\begin{aligned}
 U_{ij}^l &= \mathbb{E}_z \left[ \varrho \left( \frac{w_i^T(ax_l + \sqrt{h}z)}{\sqrt{d}} \right) \varrho \left( \frac{w_j^T(ax_l + \sqrt{h}z)}{\sqrt{d}} \right) \right] \\
 &= \mathbb{E}_{(u,v) \sim P^{\frac{w_i^T w_j}{d}}} \left[ \varrho \left( a \frac{w_i^T x_l}{\sqrt{d}} + \sqrt{h}u \right) \varrho \left( a \frac{w_j^T x_l}{\sqrt{d}} + \sqrt{h}v \right) \right] \\
 &= \sum_{k=0}^{\infty} \frac{\left( \frac{w_i^T w_j}{d} \right)^k}{k!} \mathbb{E}_u \left[ \varrho \left( a \frac{w_i^T x_l}{\sqrt{d}} + \sqrt{h}u \right) \mathbf{He}_k(u) \right] \mathbb{E}_v \left[ \varrho \left( a \frac{w_j^T x_l}{\sqrt{d}} + \sqrt{h}v \right) \mathbf{He}_k(v) \right] \\
 &= \varrho_0 \left( a \frac{w_i^T x_l}{\sqrt{d}} \right) \varrho_0 \left( a \frac{w_j^T x_l}{\sqrt{d}} \right) + \frac{w_i^T w_j}{d} \varrho_1 \left( a \frac{w_i^T x_l}{\sqrt{d}} \right) \varrho_1 \left( a \frac{w_j^T x_l}{\sqrt{d}} \right) + O(1/d),
 \end{aligned}$$

where  $\varrho_0(y) = \mathbb{E}_u [\varrho(y + \sqrt{h}u)]$  and  $\varrho_1(y) = \mathbb{E}_u [\varrho(y + \sqrt{h}u)u]$ . Summing over the  $n$  data samples:

$$\begin{aligned}
 U_{ij} &= \frac{1}{n} \sum_{l=1}^n U_{ij}^l \\
 &= \frac{1}{n} \sum_{l=1}^n \varrho_0 \left( a \frac{w_i^T x_l}{\sqrt{d}} \right) \varrho_0 \left( a \frac{w_j^T x_l}{\sqrt{d}} \right) + \frac{w_i^T w_j}{d} \frac{1}{n} \sum_{l=1}^n \varrho_1 \left( a \frac{w_i^T x_l}{\sqrt{d}} \right) \varrho_1 \left( a \frac{w_j^T x_l}{\sqrt{d}} \right) + O(1/d) \\
 &= \frac{1}{n} \sum_{l=1}^n \varrho_0 \left( a \frac{w_i^T x_l}{\sqrt{d}} \right) \varrho_0 \left( a \frac{w_j^T x_l}{\sqrt{d}} \right) + \frac{w_i^T w_j}{d} \mathbb{E}_x \left[ \varrho_1 \left( a \frac{w_i^T x}{\sqrt{d}} \right) \varrho_1 \left( a \frac{w_j^T x}{\sqrt{d}} \right) \right] + O(1/d) \\
 &= \frac{1}{n} \sum_{l=1}^n \varrho_0 \left( a \frac{w_i^T x_l}{\sqrt{d}} \right) \varrho_0 \left( a \frac{w_j^T x_l}{\sqrt{d}} \right) + \frac{w_i^T w_j}{d} \mathbb{E}_g [\varrho_1(ag)]^2 + O(1/d) \\
 &= \frac{1}{n} \sum_{l=1}^n \varrho_0 \left( a \frac{w_i^T x_l}{\sqrt{d}} \right) \varrho_0 \left( a \frac{w_j^T x_l}{\sqrt{d}} \right) + h\mu_1^2 \frac{w_i^T w_j}{d} + O(1/d).
 \end{aligned}$$

For  $i = j$ , we have:

$$U_{ii}^l = \mathbb{E}_z \left[ \left( \varrho \left( \frac{w_i^T (ax_l + \sqrt{h}z)}{\sqrt{d}} \right) \right)^2 \right],$$

and

$$\begin{aligned} U_{ii} &= \frac{1}{n} \sum_{l=1}^n \mathbb{E}_z \left[ \left( \varrho \left( \frac{w_i^T (ax_l + \sqrt{h}z)}{\sqrt{d}} \right) \right)^2 \right] \\ &= \mathbb{E}_{z,x} \left[ \left( \varrho \left( \frac{w_i^T (ax_l + \sqrt{h}z)}{\sqrt{d}} \right) \right)^2 \right] + O(1/\sqrt{d}) \\ &= \|\varrho\|^2 + O(1/\sqrt{d}). \end{aligned}$$

The  $O(1/\sqrt{d})$  term in the above equation can be neglected, since there are only  $O(d)$  terms on the diagonal. Let  $X = [x_1, x_2, \dots, x_n] \in \mathbb{R}^{d \times n}$ . We can write  $U$  as:

$$U = \frac{\varrho_0 \left( a \frac{W}{\sqrt{d}} X \right)}{\sqrt{n}} \frac{\varrho_0 \left( a \frac{W}{\sqrt{d}} X \right)^T}{\sqrt{n}} + h\mu_1^2 \frac{W}{\sqrt{d}} \frac{W^T}{\sqrt{d}} + s^2 I_p,$$

where

$$\begin{aligned} s^2 &= \|\varrho\|^2 - \mathbb{E}_g [\varrho_0(ag)^2] - h\mu_1^2 \\ &= \|\varrho\|^2 - \mathbb{E}_g \left[ \mathbb{E}_u [\varrho(ag + \sqrt{h}u)]^2 \right] - h\mu_1^2 \\ &= \|\varrho\|^2 - c(a^2) - h\mu_1^2, \end{aligned}$$

with  $c(\gamma) = \mathbb{E}_{u,v \sim P_\gamma} [\varrho(u)\varrho(v)]$ .

We can use Gaussian equivalence principle to replace the nonlinear term in  $U$ . A Gaussian equivalent for  $\varrho_0(a \frac{W}{\sqrt{d}} X)$  is given by

$$\begin{aligned} G &= \mathbb{E}_g [\varrho_0(ag)] \mathbf{1}_p \mathbf{1}_n^T + \mathbb{E}_g [\varrho_0(ag)g] \frac{W}{\sqrt{d}} X + \left( \mathbb{E}_g [\varrho_0(ag)^2] - \mathbb{E}_g [\varrho_0(ag)]^2 - \mathbb{E}_g [\varrho_0(ag)g]^2 \right)^{1/2} \Omega \\ &= \mu_0 \mathbf{1}_p \mathbf{1}_n^T + a\mu_1 \frac{W}{\sqrt{d}} X + \underbrace{\left( c(a^2) - \mu_0^2 - a^2 \mu_1^2 \right)}_{:=v_0^2} \Omega, \end{aligned}$$

where  $\Omega \in \mathbb{R}^{p \times n}$  is a random matrix with standard Gaussian entries. Hence we have

$$U = \frac{G}{\sqrt{n}} \frac{G^T}{\sqrt{n}} + h\mu_1^2 \frac{W}{\sqrt{d}} \frac{W^T}{\sqrt{d}} + s^2 I_p,$$

with

$$G = \mu_0 \mathbf{1}_p \mathbf{1}_n^T + a\mu_1 \frac{W}{\sqrt{d}} X + v_0 \Omega.$$

We now have expressions for all terms in the generalization error.

$$\begin{aligned} \mathcal{E}_{\text{test}}^\infty(\hat{A}_t) &= 1 - \frac{2}{d} \text{tr} \left\{ \frac{1}{\sqrt{h}} V^T (U + \lambda I_p)^{-1} \tilde{V} \right\} + \frac{1}{d} \text{tr} \left\{ \frac{1}{h} (U + \lambda I_p)^{-1} V V^T (U + \lambda I_p)^{-1} \tilde{U} \right\} \\ &= 1 - \frac{2\mu_1^2}{d} \text{tr} \left\{ \frac{W^T}{\sqrt{d}} (U + \lambda I_p)^{-1} \frac{W}{\sqrt{d}} \right\} \\ &\quad + \frac{\mu_1^2}{d} \text{tr} \left\{ (U + \lambda I_p)^{-1} \frac{W}{\sqrt{d}} \frac{W^T}{\sqrt{d}} (U + \lambda I_p)^{-1} \left( \mu_0^2 \mathbf{1}_p \mathbf{1}_p^T + \mu_1^2 \frac{W}{\sqrt{d}} \frac{W^T}{\sqrt{d}} + v^2 I_p \right) \right\}. \end{aligned}$$



For simplicity in presentation, assume that  $\mu_0 = 0$  and write

$$\mathcal{E}_{\text{test}}^\infty(\hat{A}_t) = 1 - 2\mu_1^2 E_1 + \mu_1^4 E_2 + \mu_1^2 v^2 E_3 ,$$

with

$$\begin{aligned} E_1 &= \frac{1}{d} \text{tr} \left\{ \frac{W^T}{\sqrt{d}} (U + \lambda I_p)^{-1} \frac{W}{\sqrt{d}} \right\} , \\ E_2 &= \frac{1}{d} \text{tr} \left\{ \frac{W^T}{\sqrt{d}} (U + \lambda I_p)^{-1} \frac{W}{\sqrt{d}} \frac{W^T}{\sqrt{d}} (U + \lambda I_p)^{-1} \frac{W}{\sqrt{d}} \right\} , \\ E_3 &= \frac{1}{d} \text{tr} \left\{ \frac{W^T}{\sqrt{d}} (U + \lambda I_p)^{-2} \frac{W}{\sqrt{d}} \right\} . \end{aligned}$$

Now define the following matrix

$$U(q) := \frac{G}{\sqrt{n}} \frac{G^T}{\sqrt{n}} + (h\mu_1^2 + q) \frac{W}{\sqrt{d}} \frac{W^T}{\sqrt{d}} + s^2 I_p ,$$

and the resolvent of  $U(q)$  as

$$R(q, z) = (U(q) - zI_p)^{-1} .$$

Let

$$K(q, z) = \frac{1}{d} \text{tr} \left\{ \frac{W^T}{\sqrt{d}} R(q, z) \frac{W}{\sqrt{d}} \right\} .$$

Using the identities  $\frac{\partial R}{\partial q} = -R(q, z) \frac{dU}{dq} R(q, z)$  and  $\frac{\partial R}{\partial z} = R(q, z)^2$ , we observe that

$$\begin{aligned} E_1 &= K(0, -\lambda) , \\ E_2 &= -\frac{\partial K}{\partial q}(0, -\lambda) , \\ E_3 &= \frac{\partial K}{\partial z}(0, -\lambda) . \end{aligned}$$

Therefore, assuming we can take limit of the expectation inside the derivative, it suffices to have the function  $\mathcal{K}(q, z) := \lim_{d \rightarrow \infty} \mathbb{E}[K(q, z)]$  to have an expression for  $\lim_{d \rightarrow \infty} \mathbb{E}[\mathcal{E}_{\text{test}}^\infty(\hat{A}_t)]$ . We have

$$\begin{aligned} \lim_{d \rightarrow \infty} \mathbb{E} \left[ \mathcal{E}_{\text{test}}^\infty(\hat{A}_t) \right] &= 1 - 2\mu_1^2 \lim_{d \rightarrow \infty} \mathbb{E}[E_1] + \mu_1^4 \lim_{d \rightarrow \infty} \mathbb{E}[E_2] + \mu_1^2 v^2 \lim_{d \rightarrow \infty} \mathbb{E}[E_3] , \\ &= 1 - 2\mu_1^2 \mathcal{K}(0, -\lambda) + \mu_1^4 \frac{\partial \mathcal{K}}{\partial q}(0, -\lambda) + \mu_1^2 v^2 \frac{\partial \mathcal{K}}{\partial z}(0, -\lambda) , \\ &= 1 - 2\mu_1^2 e_1 + \mu_1^4 e_2 + \mu_1^2 v^2 e_3 , \end{aligned} \tag{13}$$

where we define  $e_1 = \mathcal{K}(0, -\lambda)$ ,  $e_2 = -\frac{\partial \mathcal{K}}{\partial q}(0, -\lambda)$ ,  $e_3 = \frac{\partial \mathcal{K}}{\partial z}(0, -\lambda)$ . The above computations can also be performed avoiding the change in order of derivatives and expectation, by first differentiating  $K(q, z)$  (instead of  $\mathcal{K}(q, z)$ ), and then constructing a linear pencil matrix that is almost twice the size of the current one. This is more tedious, and we opt for the smaller linear pencil matrix here.

We derive an expression for  $\mathcal{K}$  using the Linear Pencils method. We start by constructing the following  $4 \times 4$  block matrix:

$$L = \left[ \begin{array}{c|ccc} (s^2 - z)I_p & a\mu_1 \frac{W}{\sqrt{d}} & v_0 \frac{\Omega}{\sqrt{n}} & (h\mu_1^2 + q) \frac{W}{\sqrt{d}} \\ \hline 0 & I_d & -\frac{X}{\sqrt{n}} & 0 \\ -v_0 \frac{\Omega^T}{\sqrt{n}} & 0 & I_n & -a\mu_1 \frac{X^T}{\sqrt{n}} \\ -\frac{W^T}{\sqrt{d}} & 0 & 0 & I_d \end{array} \right] = \begin{bmatrix} L_{11} & L_{12} \\ L_{21} & L_{22} \end{bmatrix} .$$

First, we can invert  $L$  and verify that  $K$  is trace of one of the blocks in  $L^{-1}$ . Let  $\bar{L}_{22} = L_{11} - L_{12} L_{22}^{-1} L_{21}$ . Using the block matrix inversion formula, we have:

$$L^{-1} = \begin{bmatrix} \bar{L}_{22}^{-1} & -\bar{L}_{22}^{-1} L_{12} L_{22}^{-1} \\ -L_{22}^{-1} L_{21} \bar{L}_{22}^{-1} & L_{22}^{-1} + L_{22}^{-1} L_{21} \bar{L}_{22}^{-1} L_{12} L_{22}^{-1} \end{bmatrix} ,$$

$$L_{22}^{-1} = \begin{bmatrix} I_d & \frac{X}{\sqrt{n}} & a\mu_1 \frac{X}{\sqrt{n}} \frac{X^T}{\sqrt{n}} \\ 0 & I_n & a\mu_1 \frac{X^T}{\sqrt{n}} \\ 0 & 0 & I_d \end{bmatrix},$$

$$\begin{aligned} \bar{L}_{22} &= (s^2 - z)I_p + v_0 \frac{G}{\sqrt{n}} \frac{\Omega^T}{\sqrt{n}} + a\mu_1 \frac{G}{\sqrt{n}} \frac{X^T}{\sqrt{n}} \frac{W^T}{\sqrt{d}} + (h\mu_1^2 + q) \frac{W}{\sqrt{d}} \frac{W^T}{\sqrt{d}} \\ &= (s^2 - z)I_p + \frac{G}{\sqrt{n}} \frac{G^T}{\sqrt{n}} + (h\mu_1^2 + q) \frac{W}{\sqrt{d}} \frac{W^T}{\sqrt{d}} \\ &= R^{-1}(q, z). \end{aligned}$$

Hence,

$$L^{-1} = \begin{bmatrix} R(q, z) & -a\mu_1 R(q, z) \frac{W}{\sqrt{d}} & -R(q, z) \frac{G}{\sqrt{n}} & & & \\ \frac{X}{\sqrt{n}} \frac{G^T}{\sqrt{n}} R(q, z) & I_d - a\mu_1 \frac{X}{\sqrt{n}} \frac{G^T}{\sqrt{n}} R(q, z) \frac{W}{\sqrt{d}} & \frac{X}{\sqrt{n}} - \frac{X}{\sqrt{n}} \frac{G^T}{\sqrt{n}} R(q, z) \frac{G}{\sqrt{n}} & & & \\ \frac{G^T}{\sqrt{n}} R(q, z) & -a\mu_1 \frac{G^T}{\sqrt{n}} R(q, z) \frac{W}{\sqrt{d}} & I_n - \frac{G^T}{\sqrt{n}} R(q, z) \frac{G}{\sqrt{n}} & & & \\ \frac{W^T}{\sqrt{d}} & -a\mu_1 \frac{W^T}{\sqrt{d}} R(q, z) \frac{W}{\sqrt{d}} & -\frac{W^T}{\sqrt{d}} R(q, z) \frac{G}{\sqrt{n}} & & & \\ & & & -R(q, z) (a\mu_1 \frac{G}{\sqrt{n}} \frac{X^T}{\sqrt{n}} + (h\mu_1^2 + q) \frac{W}{\sqrt{d}}) & & \\ & & & a\mu_1 \frac{X}{\sqrt{n}} \frac{X^T}{\sqrt{n}} - \frac{X}{\sqrt{n}} \frac{G^T}{\sqrt{n}} R(q, z) (a\mu_1 \frac{G}{\sqrt{n}} \frac{X^T}{\sqrt{n}} + (h\mu_1^2 + q) \frac{W}{\sqrt{d}}) & & \\ & & & a\mu_1 \frac{X^T}{\sqrt{n}} - \frac{G^T}{\sqrt{n}} R(q, z) (a\mu_1 \frac{G}{\sqrt{n}} \frac{X^T}{\sqrt{n}} + (h\mu_1^2 + q) \frac{W}{\sqrt{d}}) & & \\ & & & I_d - \frac{W^T}{\sqrt{d}} R(q, z) (a\mu_1 \frac{G}{\sqrt{n}} \frac{X^T}{\sqrt{n}} + (h\mu_1^2 + q) \frac{W}{\sqrt{d}}) & & \end{bmatrix}.$$

We see that  $(L^{-1})^{4,2}$  gives the desired term. We use the linear pencil formalism to derive the traces of the square blocks in  $L^{-1}$ . Let  $g$  be the matrix of traces of square blocks in  $L^{-1}$  divided by the block size. For example, if  $L^{i,j}$  is a square matrix of dimension  $N$ , then  $g_{ij} = \frac{1}{N} \text{tr}\{(L^{-1})^{i,j}\}$ . We assign  $g_{ij} = 0$  if  $L^{i,j}$  is not a square matrix. We have

$$g = \begin{bmatrix} g_{11} & 0 & 0 & 0 \\ 0 & g_{22} & 0 & g_{24} \\ 0 & 0 & g_{33} & 0 \\ 0 & g_{42} & 0 & g_{44} \end{bmatrix}.$$

Notice that the constant matrices in  $L$  are all multiples of identity. Let  $B$  be the matrix that contains the coefficients of these constant matrices, given by

$$B = \begin{bmatrix} s^2 - z & 0 & 0 & 0 \\ 0 & 1 & 0 & 0 \\ 0 & 0 & 1 & 0 \\ 0 & 0 & 0 & 1 \end{bmatrix}.$$

If  $L^{il}$  and  $L^{jk}$  are square matrices, let  $\sigma_{ij}^{kl}$  be the covariance between an element of  $L^{ij}$  and  $L^{kl}$  multiplied by the block size of  $L^{jk}$ . Let  $L^{ij}$  be of dimension  $N_i \times N_j$  and  $M$  denote the non constant part of  $L$ . Then,

$$\sigma_{ij}^{kl} = N_j \mathbb{E}[M_{uv}^{ij} M_{vu}^{kl}].$$

Let  $S = \{(i, j) : N_i = N_j\}$  be the set of indices of square blocks in  $L$ . Then, a mapping  $\eta_L$  is defined such that

$$\eta_L(G)_{il} = \sum_{(jk) \in S} \sigma_{ij}^{kl} g_{jk},$$

for  $(il)$  in  $S$ . We get

$$\eta_L(g) = \begin{bmatrix} \sigma_{12}^{41} g_{24} + \sigma_{13}^{31} g_{33} + \sigma_{14}^{41} g_{44} & 0 & 0 & 0 \\ 0 & 0 & 0 & \sigma_{23}^{34} g_{33} \\ 0 & 0 & \sigma_{31}^{13} g_{11} + \sigma_{34}^{23} g_{42} & 0 \\ 0 & \sigma_{41}^{12} g_{11} & 0 & \sigma_{41}^{14} g_{11} \end{bmatrix}.$$

We have  $N_1 = p, N_2 = d, N_3 = n, N_4 = d$ :

$$\sigma_{12}^{41} = -a\mu_1, \quad \sigma_{41}^{12} = -a\mu_1\psi_p, \quad (14)$$

$$\sigma_{13}^{31} = -v_0^2, \quad \sigma_{31}^{13} = -v_0^2\psi_p/\psi_n, \quad (15)$$

$$\sigma_{14}^{41} = -(h\mu_1^2 + q), \quad \sigma_{41}^{14} = -(h\mu_1^2 + q)\psi_p, \quad (16)$$

$$\sigma_{23}^{34} = a\mu_1, \quad \sigma_{34}^{23} = a\mu_1/\psi_n. \quad (17)$$

We have that  $g$  satisfies the following fixed point equation

$$(B - \eta_L(g))g = I.$$

Hence:

$$\begin{bmatrix} s^2 - z + a\mu_1g_{24} + v_0^2g_{33} + (h\mu_1^2 + q)g_{44} & 0 & 0 & 0 \\ 0 & 1 & 0 & -a\mu_1g_{33} \\ 0 & 0 & 1 + v_0^2\psi_p/\psi_n g_{11} - a\mu_1/\psi_n g_{42} & 0 \\ 0 & a\mu_1\psi_p g_{11} & 0 & 1 + (h\mu_1^2 + q)\psi_p g_{11} \end{bmatrix} \times \begin{bmatrix} g_{11} & 0 & 0 & 0 \\ 0 & g_{22} & 0 & g_{24} \\ 0 & 0 & g_{33} & 0 \\ 0 & g_{42} & 0 & g_{44} \end{bmatrix} = I.$$

This gives the following set of equations:

$$\begin{aligned} g_{11}(s^2 - z + a\mu_1g_{24} + v_0^2g_{33} + (h\mu_1^2 + q)g_{44}) &= 1, \\ g_{22} - a\mu_1g_{33}g_{42} &= 1, \\ g_{24} - a\mu_1g_{33}g_{44} &= 0, \\ g_{33}(1 + v_0^2\psi_p/\psi_n g_{11} - a\mu_1/\psi_n g_{42}) &= 1, \\ a\mu_1\psi_p g_{11}g_{22} + (1 + (h\mu_1^2 + q)\psi_p g_{11})g_{42} &= 0, \\ a\mu_1\psi_p g_{11}g_{24} + (1 + (h\mu_1^2 + q)\psi_p g_{11})g_{44} &= 1, \end{aligned}$$

The above set of 6 equations can be reduced to the following set of 4 equations:

$$\begin{aligned} \zeta_1(s^2 - z + a_t^2\mu_1^2\zeta_2\zeta_4 + v_0^2\zeta_2 + (h_t\mu_1^2 + q)\zeta_4) - 1 &= 0, \\ \zeta_2(\psi_n + v_0^2\psi_p\zeta_1 - a_t\mu_1\zeta_3) - \psi_n &= 0, \\ a_t\mu_1\psi_p\zeta_1(1 + a_t\mu_1\zeta_2\zeta_3) + (1 + (h_t\mu_1^2 + q)\psi_p\zeta_1)\zeta_3 &= 0, \\ a_t^2\mu_1^2\psi_p\zeta_1\zeta_2\zeta_4 + (1 + (h_t\mu_1^2 + q)\psi_p\zeta_1)\zeta_4 - 1 &= 0, \end{aligned}$$

where  $\zeta_1 = g_{11}$ ,  $\zeta_2 = g_{33}$ ,  $\zeta_3 = g_{42}$ ,  $\zeta_4 = g_{44}$ . We solve the above set of equations numerically to obtain  $\zeta_1, \zeta_2, \zeta_3$ , and  $\zeta_4$ . We compute  $\mathcal{K} = \lim_{d \rightarrow \infty} \mathbb{E}[K]$  by using the expression  $\mathcal{K}(q, z) = -\frac{\zeta_3(q, z)}{a\mu_1}$ . Finally, we use (13) to compute  $\lim_{d \rightarrow \infty} \mathbb{E}[\mathcal{E}_{\text{test}}^\infty(\hat{A}_t)]$ .

Next, we look at the train error.

**Train error:**

$$\begin{aligned}
 \mathcal{E}_{\text{train}}^\infty(\hat{A}_t) &= \mathcal{L}(\hat{A}) - \frac{h_t \lambda}{pd} \left\| \hat{A} \right\|_F^2 \\
 &= \frac{h}{d} \text{tr} \left\{ \frac{\hat{A}_t^T}{\sqrt{p}} \frac{\hat{A}_t}{\sqrt{p}} (U + \lambda I_p) \right\} + \frac{2\sqrt{h}}{d} \text{tr} \left\{ \frac{\hat{A}_t}{\sqrt{p}} V \right\} + 1 - \frac{h\lambda}{d} \text{tr} \left\{ \frac{\hat{A}_t^T}{\sqrt{p}} \frac{\hat{A}_t}{\sqrt{p}} \right\} \\
 &= \frac{1}{d} \text{tr} \{ (U + \lambda I_p)^{-1} V V^T \} - \frac{2}{d} \text{tr} \{ V^T (U + \lambda I_p)^{-1} V \} + 1 - \frac{\lambda}{d} \text{tr} \{ V^T (U + \lambda I_p)^{-2} V \} \\
 &= -\frac{h\mu_1^2}{d} \text{tr} \left\{ (U + \lambda I_p)^{-1} \frac{W}{\sqrt{d}} \frac{W^T}{\sqrt{d}} \right\} + 1 - \frac{h\mu_1^2 \lambda}{d} \text{tr} \left\{ (U + \lambda I_p)^{-2} \frac{W}{\sqrt{d}} \frac{W^T}{\sqrt{d}} \right\} \\
 &= -h\mu_1^2 K(0, -\lambda) - h\lambda\mu_1^2 \frac{\partial K}{\partial z}(0, -\lambda) + 1.
 \end{aligned}$$

Thus,

$$\begin{aligned}
 \lim_{d \rightarrow \infty} \mathbb{E} \left[ \mathcal{E}_{\text{train}}^\infty(\hat{A}_t) \right] &= -h\mu_1^2 K(0, -\lambda) - h\lambda\mu_1^2 \frac{\partial K}{\partial z}(0, -\lambda) + 1, \\
 &= 1 - h\mu_1^2 e_1 - h\lambda\mu_1^2 e_3,
 \end{aligned} \tag{18}$$

where  $e_1 = K(0, -\lambda)$ ,  $e_3 = \frac{\partial K}{\partial z}(0, -\lambda)$ . This concludes the proof of Theorem 3.2.

### C. Proof of Theorem 3.5

When  $m = 1$ , the loss function reduces to:

$$\mathcal{L}_t^1(A_t) = \frac{1}{dn} \sum_{i=1}^n \left\| \sqrt{h_t} \frac{A_t}{\sqrt{p}} \varrho \left( \frac{W_t}{\sqrt{p}} (a_t x_i + \sqrt{h_t} z_i) \right) + z_i \right\|^2 + \frac{h_t \lambda}{dp} \|A_t\|_F^2. \tag{19}$$

Let  $X = [x_1, x_2, \dots, x_n]$ ,  $Z = [z_1, z_2, \dots, z_n]$ , and let  $Y$  be a matrix with its  $i^{\text{th}}$  column given as  $y_i = a_t x_i + \sqrt{h_t} z_i$ . Also let  $F = \varrho \left( \frac{W}{\sqrt{d}} Y \right)$ . We then write:

$$\begin{aligned}
 \mathcal{L}_t^1(A_t) &= \frac{1}{dn} \sum_{i=1}^n \left\| \sqrt{h_t} \frac{A_t}{\sqrt{p}} \varrho \left( \frac{W_t}{\sqrt{p}} (a_t x_i + \sqrt{h_t} z_i) \right) + z_i \right\|^2 + \frac{h_t \lambda}{dp} \|A_t\|_F^2 \\
 &= \frac{h_t}{d} \text{tr} \left\{ \frac{A_t^T}{\sqrt{p}} \frac{A_t}{\sqrt{p}} U \right\} + \frac{2\sqrt{h_t}}{d} \text{tr} \left\{ \frac{A_t}{\sqrt{p}} V \right\} + 1 + \frac{h_t \lambda}{d} \text{tr} \left\{ \frac{A_t^T}{\sqrt{p}} \frac{A_t}{\sqrt{p}} \right\},
 \end{aligned}$$

where

$$U = \frac{1}{n} \varrho \left( \frac{W_t}{\sqrt{d}} Y \right) \varrho \left( \frac{W_t}{\sqrt{d}} Y \right)^T = \frac{F}{\sqrt{n}} \frac{F^T}{\sqrt{n}},$$

and

$$V = \frac{1}{n} \varrho \left( \frac{W_t}{\sqrt{d}} Y \right) Z^T = \frac{F}{\sqrt{n}} \frac{Z^T}{\sqrt{n}}.$$

Thus we get the optimal  $A_t$  as

$$\frac{\hat{A}_t}{\sqrt{p}} = -\frac{1}{\sqrt{h_t}} V^T (U + \lambda I_p)^{-1} = -\frac{1}{\sqrt{h_t}} \frac{Z}{\sqrt{n}} \frac{F^T}{\sqrt{n}} \left( \frac{F}{\sqrt{n}} \frac{F^T}{\sqrt{n}} + \lambda I_p \right)^{-1}. \tag{20}$$



**Test error:**

$$\begin{aligned}
 \mathcal{E}_{\text{test}}^1(\hat{A}_t) &= \frac{1}{d} \mathbb{E}_{x \sim P_t} \left[ \left\| \frac{\hat{A}_t}{\sqrt{p}} \varrho \left( \frac{W_t}{\sqrt{d}} x \right) - \nabla \log P_t(x) \right\|^2 \right] \\
 &= \frac{1}{d} \mathbb{E}_{x \sim P_t} \left[ \left\| \frac{\hat{A}_t}{\sqrt{p}} \varrho \left( \frac{W_t}{\sqrt{d}} x \right) + x \right\|^2 \right] \\
 &= 1 + \frac{2}{d} \text{tr} \left\{ \frac{\hat{A}_t}{\sqrt{p}} \underbrace{\mathbb{E}_x \left[ \varrho \left( \frac{W_t}{\sqrt{d}} x \right) x^T \right]}_{:= \tilde{V}} \right\} + \frac{1}{d} \text{tr} \left\{ \frac{\hat{A}_t^T}{\sqrt{p}} \frac{\hat{A}_t}{\sqrt{p}} \underbrace{\mathbb{E}_x \left[ \varrho \left( \frac{W_t}{\sqrt{d}} x \right) \varrho \left( \frac{W_t}{\sqrt{d}} x \right)^T \right]}_{:= \tilde{U}} \right\}.
 \end{aligned}$$

We have already derived expressions for  $\tilde{V}$  and  $\tilde{U}$  in Section B. We have  $\tilde{V} = \mu_1 \frac{W}{\sqrt{d}}$ ,  $\tilde{U} = \mu_0^2 \mathbf{1}\mathbf{1}^T + \mu_1^2 \frac{W}{\sqrt{d}} \frac{W^T}{\sqrt{d}} + v^2 I_p$ . For simplicity, we assume  $\mu_0 = 0$ . Thus:

$$\begin{aligned}
 \mathcal{E}_{\text{test}}^1(\hat{A}_t) &= \frac{1}{d} \mathbb{E}_{x \sim P_t} \left[ \left\| \frac{\hat{A}_t}{\sqrt{p}} \varrho \left( \frac{W_t}{\sqrt{d}} x \right) + x \right\|^2 \right] \\
 &= 1 - \frac{2\mu_1}{\sqrt{h_t d}} \text{tr} \left\{ \frac{Z}{\sqrt{n}} \frac{F^T}{\sqrt{n}} \left( \frac{F}{\sqrt{n}} \frac{F^T}{\sqrt{n}} + \lambda I_p \right)^{-1} \frac{W}{\sqrt{d}} \right\} \\
 &\quad + \frac{\mu_1^2}{h_t d} \text{tr} \left\{ \left( \frac{F}{\sqrt{n}} \frac{F^T}{\sqrt{n}} + \lambda I_p \right)^{-1} \frac{F}{\sqrt{n}} \frac{Z^T}{\sqrt{n}} \frac{Z}{\sqrt{n}} \frac{F^T}{\sqrt{n}} \left( \frac{F}{\sqrt{n}} \frac{F^T}{\sqrt{n}} + \lambda I_p \right)^{-1} \frac{W}{\sqrt{d}} \frac{W^T}{\sqrt{d}} \right\} \\
 &\quad + \frac{v^2}{h_t d} \text{tr} \left\{ \left( \frac{F}{\sqrt{n}} \frac{F^T}{\sqrt{n}} + \lambda I_p \right)^{-1} \frac{F}{\sqrt{n}} \frac{Z^T}{\sqrt{n}} \frac{Z}{\sqrt{n}} \frac{F^T}{\sqrt{n}} \left( \frac{F}{\sqrt{n}} \frac{F^T}{\sqrt{n}} + \lambda I_p \right)^{-1} \right\}.
 \end{aligned}$$

Since we focus on a single time instant, we have dropped the subscript  $t$  in the above expressions. However, it is important to keep the time-dependence of  $a$  and  $h$ , and the relation  $a^2 + h = 1$ . Also, we use Gaussian equivalence principle to handle the non-linearity in  $F$ . In particular, we use the following expression for  $F$ :

$$F = \mu_1 \frac{W}{\sqrt{d}} Y + v \Omega.$$

Let

$$R(q, z) = \left( \frac{F}{\sqrt{n}} \frac{F^T}{\sqrt{n}} + q \frac{W}{\sqrt{d}} \frac{W^T}{\sqrt{d}} - z I_p \right)^{-1}, \quad (21)$$

and

$$\begin{aligned}
 E_1 &= \frac{1}{d} \text{tr} \left\{ \frac{Z}{\sqrt{n}} \frac{F^T}{\sqrt{n}} R(0, -\lambda) \frac{W}{\sqrt{d}} \right\}, \\
 E_2 &= \frac{1}{d} \text{tr} \left\{ R(0, -\lambda) \frac{F}{\sqrt{n}} \frac{Z^T}{\sqrt{n}} \frac{Z}{\sqrt{n}} \frac{F^T}{\sqrt{n}} R(0, -\lambda) \frac{W}{\sqrt{d}} \frac{W^T}{\sqrt{d}} \right\}, \\
 E_3 &= \frac{1}{d} \text{tr} \left\{ \frac{F}{\sqrt{n}} \frac{Z^T}{\sqrt{n}} \frac{Z}{\sqrt{n}} \frac{F^T}{\sqrt{n}} R(0, -\lambda)^2 \right\}.
 \end{aligned}$$

With above definitions, we can write  $\mathcal{E}_{\text{test}}^1$  as

$$\mathcal{E}_{\text{test}}^1(\hat{A}_t) = 1 - \frac{2\mu_1}{\sqrt{h}} E_1 + \frac{\mu_1^2}{h} E_2 + \frac{v^2}{h} E_3.$$

Letting

$$K(q, z) = \frac{1}{d} \operatorname{tr} \left\{ R(q, z) \frac{F}{\sqrt{n}} \frac{Z^T}{\sqrt{n}} \frac{Z}{\sqrt{n}} \frac{F^T}{\sqrt{n}} \right\},$$

we have

$$\begin{aligned} E_2 &= -\frac{dK}{dq}(0, -\lambda), \\ E_3 &= \frac{dK}{dz}(0, -\lambda). \end{aligned}$$

Therefore, assuming we can interchange limit, derivatives and expectations, it suffices to have  $e_1 = \lim_{d \rightarrow \infty} \mathbb{E}[E_1]$  and the function  $\mathcal{K}(q, z) := \lim_{d \rightarrow \infty} \mathbb{E}[K(q, z)]$  to have an expression for  $\lim_{d \rightarrow \infty} \mathbb{E}[\mathcal{E}_{\text{test}}^1(\hat{A}_t)]$ . We have

$$\begin{aligned} \lim_{d \rightarrow \infty} \mathbb{E}[\mathcal{E}_{\text{test}}^1(\hat{A}_t)] &= 1 - \frac{2\mu_1}{\sqrt{h}} \lim_{d \rightarrow \infty} \mathbb{E}[E_1] + \frac{\mu_1^2}{h} \lim_{d \rightarrow \infty} \mathbb{E}[E_2] + \frac{v^2}{h} \lim_{d \rightarrow \infty} \mathbb{E}[E_3], \\ &= 1 - \frac{2\mu_1}{\sqrt{h}} e_1 + \frac{\mu_1^2}{h} e_2 + \frac{v^2}{h} e_3, \end{aligned} \quad (22)$$

where we define  $e_2 = -\frac{\partial K}{\partial q}(0, -\lambda)$ ,  $e_3 = \frac{\partial K}{\partial z}(0, -\lambda)$ . As in the previous theorem one could avoid the interchange of limit of expectation and derivatives by differentiating first  $K(q, z)$  and using a larger linear pencil.

As in the proof of Theorem 3.2 given in Appendix B, we use linear pencils to obtain the desired terms. Explicitly, the following  $6 \times 6$  linear pencil matrix:

$$L = \left[ \begin{array}{c|cccccc} -zI_p & q \frac{W}{\sqrt{d}} & v_0 \frac{\Omega}{\sqrt{n}} & \mu_1 \frac{W}{\sqrt{d}} & 0 & 0 \\ \hline -\frac{W^T}{\sqrt{d}} & I_d & 0 & 0 & 0 & 0 \\ -v \frac{\Omega^T}{\sqrt{n}} & -\mu \frac{Y^T}{\sqrt{n}} & I_n & 0 & 0 & 0 \\ 0 & 0 & -\frac{Y}{\sqrt{n}} & I_d & 0 & 0 \\ 0 & 0 & -\frac{Z}{\sqrt{n}} & 0 & I_d & 0 \\ 0 & 0 & 0 & 0 & -\frac{Z^T}{\sqrt{n}} & I_n \end{array} \right] = \begin{bmatrix} L_{11} & L_{12} \\ L_{21} & L_{22} \end{bmatrix}.$$

By computing  $L^{-1}$ , we obtain:

$$(L^{-1})^{5,4}(q, z) = -\mu_1 \frac{Z}{\sqrt{n}} \frac{F^T}{\sqrt{n}} R(q, z) \frac{W}{\sqrt{d}}, \quad (23)$$

$$(L^{-1})^{6,3}(q, z) = -\frac{Z^T}{\sqrt{n}} \frac{Z}{\sqrt{n}} \frac{F^T}{\sqrt{n}} R(q, z) \frac{F}{\sqrt{n}} + \frac{Z^T}{\sqrt{n}} \frac{Z}{\sqrt{n}}. \quad (24)$$

Hence,

$$E_1 = \frac{1}{d} \operatorname{tr} \left\{ \frac{Z}{\sqrt{n}} \frac{F^T}{\sqrt{n}} R(0, -\lambda) \frac{W}{\sqrt{d}} \right\} = -\frac{1}{\mu_1 d} \operatorname{tr} \{ (L^{-1})^{5,4}(0, -\lambda) \}, \quad (25)$$

$$K(q, z) = \frac{1}{d} \operatorname{tr} \left\{ R(q, z) \frac{F}{\sqrt{n}} \frac{Z^T}{\sqrt{n}} \frac{Z}{\sqrt{n}} \frac{F^T}{\sqrt{n}} \right\} = 1 - \frac{1}{d} \operatorname{tr} \{ (L^{-1})^{6,3}(q, z) \}. \quad (26)$$

We compute the traces of blocks in  $L^{-1}$  as in the proof of Theorem 3.2 given in Appendix B. We have

$$g = \begin{bmatrix} g_{11} & 0 & 0 & 0 & 0 & 0 \\ 0 & g_{22} & 0 & g_{24} & 0 & 0 \\ 0 & 0 & g_{33} & 0 & 0 & 0 \\ 0 & g_{42} & 0 & g_{44} & 0 & 0 \\ 0 & g_{52} & 0 & g_{54} & 1 & 0 \\ 0 & 0 & g_{63} & 0 & 0 & 1 \end{bmatrix}, \quad B = \begin{bmatrix} -z & 0 & 0 & 0 & 0 & 0 \\ 0 & 1 & 0 & 0 & 0 & 0 \\ 0 & 0 & 1 & 0 & 0 & 0 \\ 0 & 0 & 0 & 1 & 0 & 0 \\ 0 & 0 & 0 & 0 & 1 & 0 \\ 0 & 0 & 0 & 0 & 0 & 1 \end{bmatrix},$$

$$\eta_L(g) = \begin{bmatrix} \sigma_{12}^{21}g_{22} + \sigma_{13}^{31}g_{33} + \sigma_{14}^{21}g_{42} & 0 & 0 & 0 & 0 & 0 \\ 0 & \sigma_{21}^{12}g_{11} & 0 & \sigma_{21}^{14}g_{11} & 0 & 0 \\ 0 & 0 & \sigma_{31}^{13}g_{11} + \sigma_{32}^{43}g_{24} & 0 & 0 & 0 \\ 0 & \sigma_{43}^{32}g_{33} & 0 & 0 & 0 & 0 \\ 0 & \sigma_{53}^{32}g_{33} & 0 & 0 & 0 & 0 \\ 0 & 0 & \sigma_{65}^{43}g_{54} + \sigma_{65}^{53} & 0 & 0 & 0 \end{bmatrix},$$

and

$$\sigma_{12}^{21} = -q, \quad \sigma_{21}^{12} = -q\psi_p, \quad \sigma_{21}^{14} = -\mu_1\psi_p, \quad (27)$$

$$\sigma_{13}^{31} = -v^2, \quad \sigma_{31}^{13} = -v^2\psi_p/\psi_n, \quad \sigma_{32}^{43} = \mu_1/\psi_n, \quad \sigma_{43}^{32} = \mu_1, \quad (28)$$

$$\sigma_{14}^{21} = -\mu_1, \quad \sigma_{53}^{32} = \mu_1\sqrt{h}, \quad (29)$$

$$\sigma_{65}^{43} = \sqrt{h}/\psi_n, \quad \sigma_{65}^{53} = 1/\psi_n. \quad (30)$$

We have that  $g$  satisfies the following fixed point equation

$$(B - \eta_L(g))g = I.$$

Then:

$$\begin{bmatrix} -z + qg_{22} + v^2g_{33} + \mu_1g_{42} & 0 & 0 & 0 & 0 & 0 \\ 0 & 1 + q\psi_p g_{11} & 0 & \mu_1\psi_p g_{11} & 0 & 0 \\ 0 & 0 & 1 + v^2\psi_p/\psi_n g_{11} - \mu_1/\psi_n g_{24} & 0 & 0 & 0 \\ 0 & -\mu_1 g_{33} & 0 & 1 & 0 & 0 \\ 0 & -\mu_1\sqrt{h}g_{33} & 0 & 0 & 1 & 0 \\ 0 & 0 & -\sqrt{h}/\psi_n g_{54} - 1/\psi_n & 0 & 0 & 1 \end{bmatrix} \times \begin{bmatrix} g_{11} & 0 & 0 & 0 & 0 & 0 \\ 0 & g_{22} & 0 & g_{24} & 0 & 0 \\ 0 & 0 & g_{33} & 0 & 0 & 0 \\ 0 & g_{42} & 0 & g_{44} & 0 & 0 \\ 0 & g_{52} & 0 & g_{54} & 1 & 0 \\ 0 & 0 & g_{63} & 0 & 0 & 1 \end{bmatrix} = I.$$

This gives the following set of equations:

$$\begin{aligned} g_{11}(-z + qg_{22} + v^2g_{33} + \mu_1g_{42}) &= 1, \\ g_{22}(1 + q\psi_p g_{11}) + \mu_1\psi_p g_{11}g_{42} &= 1, \\ g_{24}(1 + q\psi_p g_{11}) + \mu_1\psi_p g_{11}g_{44} &= 0, \\ g_{33}(1 + v^2\psi_p/\psi_n g_{11} - \mu_1/\psi_n g_{24}) &= 1, \\ -\mu_1 g_{22}g_{33} + g_{42} &= 0, \\ -\mu_1 g_{24}g_{33} + g_{44} &= 1, \\ -\mu_1\sqrt{h}g_{33}g_{22} + g_{52} &= 0, \\ -\mu_1\sqrt{h}g_{33}g_{24} + g_{54} &= 0, \\ g_{33}(-\sqrt{h}/\psi_n g_{54} - 1/\psi_n) + g_{63} &= 0. \end{aligned}$$

The above set of 9 equations can be reduced to 6 equations:

$$\begin{aligned} \zeta_1(-z + q\zeta_2 + v^2\zeta_4 + \mu_1^2\zeta_2\zeta_4) - 1 &= 0, \\ \zeta_2(1 + q\psi_p\zeta_1) + \mu_1^2\psi_p\zeta_1\zeta_2\zeta_4 - 1 &= 0, \\ \zeta_3(1 + q\psi_p\zeta_1) + \mu_1\psi_p\zeta_1(1 + \mu_1\zeta_3\zeta_4) &= 0, \\ \zeta_4(\psi_n + v^2\psi_p\zeta_1 - \mu_1\zeta_3) - \psi_n &= 0, \\ \zeta_4(-h_t\mu_1\zeta_3\zeta_4 - 1) + \psi_n\zeta_5 &= 0, \end{aligned}$$

where  $\zeta_1 = g_{11}$ ,  $\zeta_2 = g_{22}$ ,  $\zeta_3 = g_{24}$ ,  $\zeta_4 = g_{33}$ ,  $\zeta_5 = g_{63}$ . As earlier, we solve the above set of equations numerically to obtain  $\zeta_1, \zeta_2, \zeta_3, \zeta_4$ , and  $\zeta_5$ . We obtain  $e_1, \mathcal{K}$  by using the expressions  $e_1 = -\sqrt{h_t}\zeta_3(0, -\lambda)\zeta_4(0, -\lambda)$ ,  $\mathcal{K}(q, z) = -\sqrt{h_t}\zeta_3(q, z)\zeta_4(q, z)$ . Finally, we use (22) to compute  $\lim_{d \rightarrow \infty} \mathbb{E}[\mathcal{E}_{\text{test}}^1(\hat{A}_t)]$ .

**Train error:** To compute train error, we proceed as follows:

$$\begin{aligned} \mathcal{E}_{\text{train}}^1(\hat{A}_t) &= \frac{h}{d} \text{tr} \left\{ \frac{\hat{A}_t^T}{\sqrt{p}} \frac{\hat{A}_t}{\sqrt{p}} (U + \lambda I_p) \right\} + \frac{2\sqrt{h}}{d} \text{tr} \left\{ \frac{\hat{A}_t}{\sqrt{p}} V \right\} + 1 - \frac{h\lambda}{d} \text{tr} \left\{ \frac{\hat{A}_t^T}{\sqrt{p}} \frac{\hat{A}_t}{\sqrt{p}} \right\} \\ &= \frac{1}{d} \text{tr} \{ (U + \lambda I_p)^{-1} V V^T \} - \frac{2}{d} \text{tr} \{ V^T (U + \lambda I_p)^{-1} V \} + 1 - \frac{\lambda}{d} \text{tr} \{ (U + \lambda I_p)^{-2} V V^T \} \\ &= -\frac{1}{d} \text{tr} \left\{ (U + \lambda I_p)^{-1} \frac{F}{\sqrt{n}} \frac{Z^T}{\sqrt{n}} \frac{Z}{\sqrt{n}} \frac{F^T}{\sqrt{n}} \right\} + 1 - \frac{\lambda}{d} \text{tr} \left\{ (U + \lambda I_p)^{-2} \frac{F}{\sqrt{n}} \frac{Z^T}{\sqrt{n}} \frac{Z}{\sqrt{n}} \frac{F^T}{\sqrt{n}} \right\} \\ &= -K(0, -\lambda) - \lambda \frac{\partial K}{\partial z}(0, -\lambda) + 1. \end{aligned}$$

Thus,

$$\begin{aligned} \lim_{d \rightarrow \infty} \mathbb{E}[\mathcal{E}_{\text{train}}^1(\hat{A}_t)] &= 1 - \mathcal{K}(0, -\lambda) - \lambda \frac{\partial \mathcal{K}}{\partial z}(0, -\lambda), \\ &= 1 - \mathcal{K}(0, -\lambda) - \lambda e_3, \end{aligned} \tag{31}$$

where  $e_3 = \frac{\partial \mathcal{K}}{\partial z}(0, -\lambda)$ . This concludes the proof of Theorem 3.5.

## D. Illustrations of Analytically Computed Test and Train Errors

In this section, we provide additional plots to further illustrate the analytical predictions of test and train errors derived from Theorems 3.2 and 3.5. First, we present the learning curves for the case of  $m = 1$ , which were omitted from the main text due to space constraints. Next, we include a plot demonstrating the impact of the regularization strength  $\lambda$  on the learning curves. Finally, we provide learning curves for cases where different activation functions are employed, highlighting their influence on the model's performance.

### D.1. Test and train errors for $m = 1$

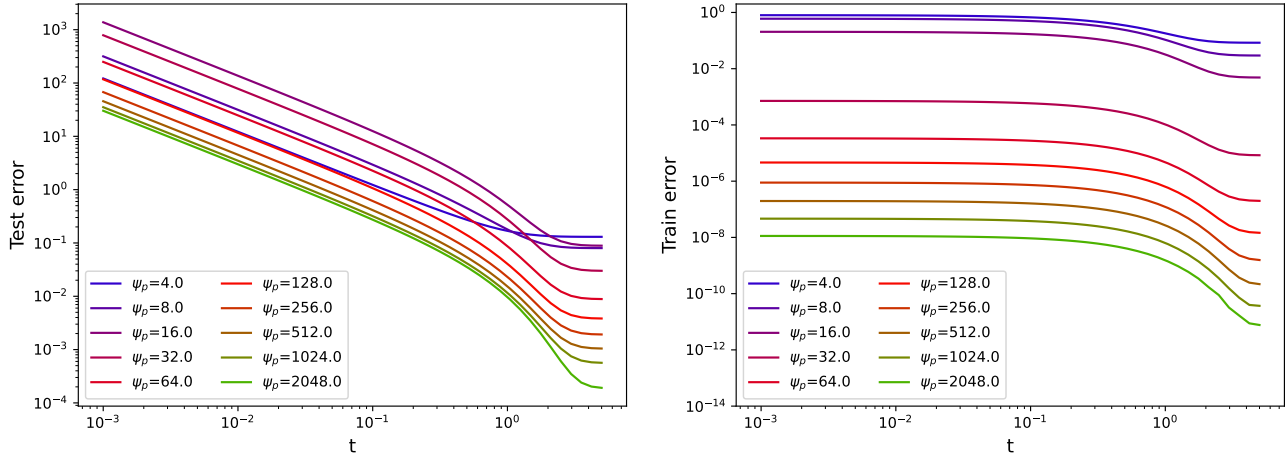
Fig. 6 shows test and train errors for  $m = 1$  case. Fig. 6a presents the learning curves as a function of  $t$  for different values of  $\psi_p$  and while keeping  $\psi_n$  fixed. In Fig. 6b we plot the learning curves as a function of  $\psi_p$  for different values of  $\psi_n$  and keeping  $t$  fixed and small.

As already discussed in the main text, the learning curves reveal several trends. The train error decreases monotonically with increasing  $\psi_p$  for all  $t$ , reflecting the model's capacity to interpolate the training data. However, the test error shows a non-monotonic behavior with  $\psi_p$ . The dependence of test error on  $t$  is also evident. The test error increases as  $t$  decreases, but for small  $t$ , it remains at least two orders of magnitude lower than in the  $m = \infty$  case. Furthermore, the test error decreases as  $\psi_p$  increases beyond  $\psi_n$ . This suggests that the model does not display memorization behavior under these conditions. This is in contrast to the  $m = \infty$  case, where memorization significantly impacts the test error. These findings indicate that larger values of  $m$  increases the tendency of diffusion models to memorize the initial dataset.

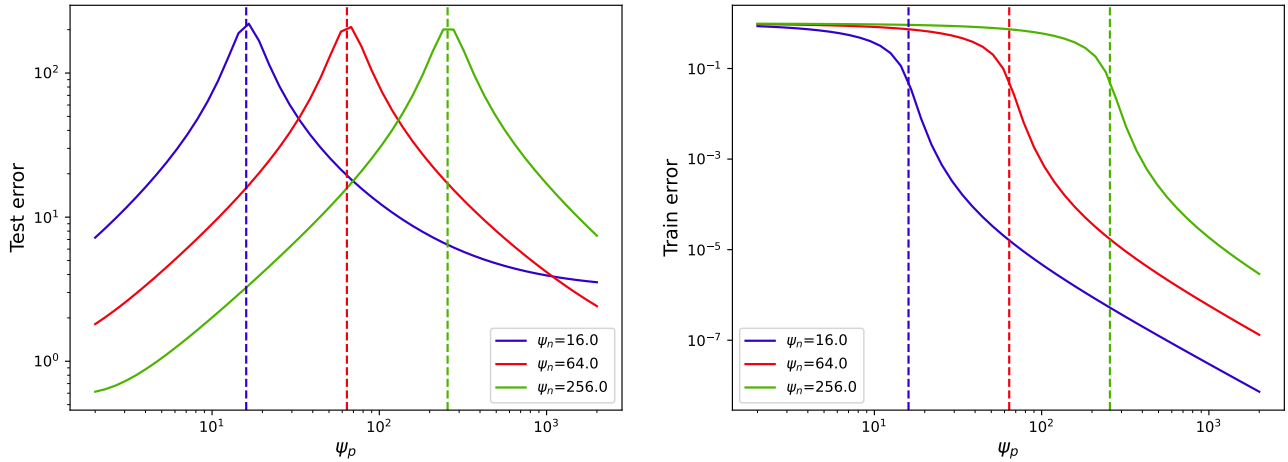
Lastly, as observed in the earlier works such as (Mei & Montanari, 2022; Bodin & Macris, 2021; Hu et al., 2024), we also observe the double descent phenomenon which is characterized by peak in test error at  $\psi_p = \psi_n$ . This is depicted in Fig. 6b.

### D.2. Plots for different values of $\lambda$

In this section, we illustrate the behavior of the test and train errors for different values of  $\lambda$ . Fig. 7 shows the learning errors for  $m = \infty$ . We see that, as  $\lambda$  increases, the train error increases and the test error decreases for small  $t$ . This can be explained as follows: In this regime, we have  $s^e(t, a_t x_i + \sqrt{h_t} z) \approx -\frac{z}{\sqrt{h_t}}$ . However, as regularization increases,  $\hat{A}_t$  cannot take very large values. So,  $\mathcal{M}_t$  scales as  $\frac{1}{h_t}$ . This makes  $\mathcal{E}_{\text{train}}^\infty(\hat{A}_t) \approx 1$  for very small values of  $t$ . This leads to lower memorization as well, as evidenced by the small test error.

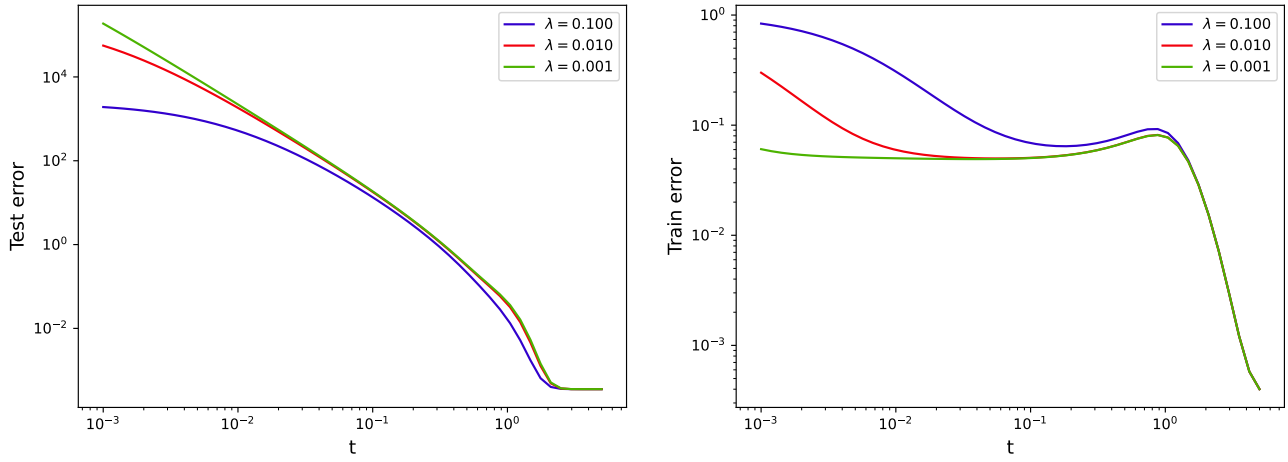


(a) Test and train error as a function of  $t$  for different values of  $\psi_p$  and a fixed  $\psi_n = 20.0$ .

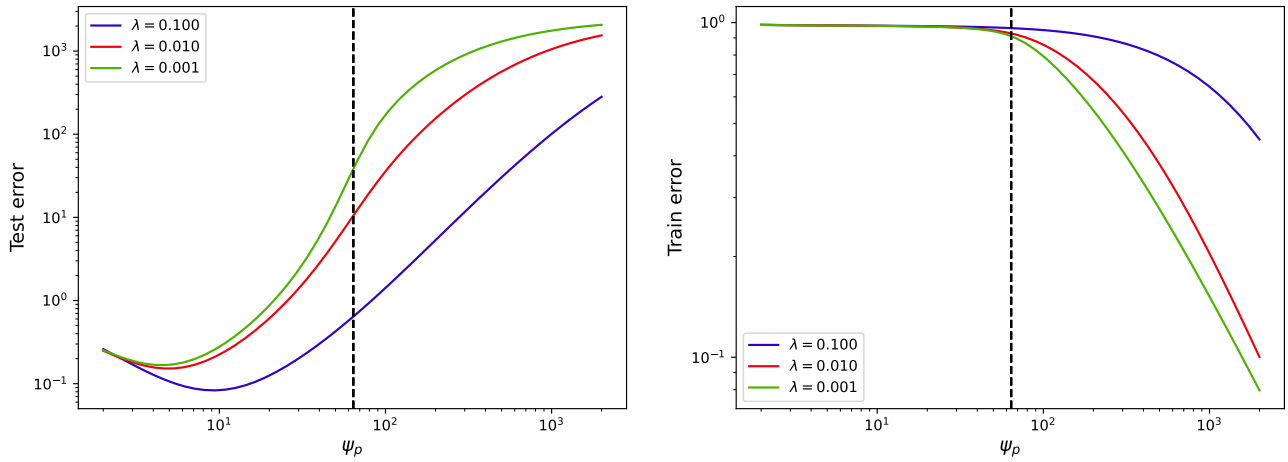


(b) Test and train error as a function of  $\psi_p$  for different values of  $\psi_n$  and a fixed  $t = 0.01$ . The dashed vertical lines indicate  $\psi_p = \psi_n$ .

Figure 6. Learning curves for  $m = 1$ . We used  $\lambda = 0.001$  and the activation function used is ReLU.

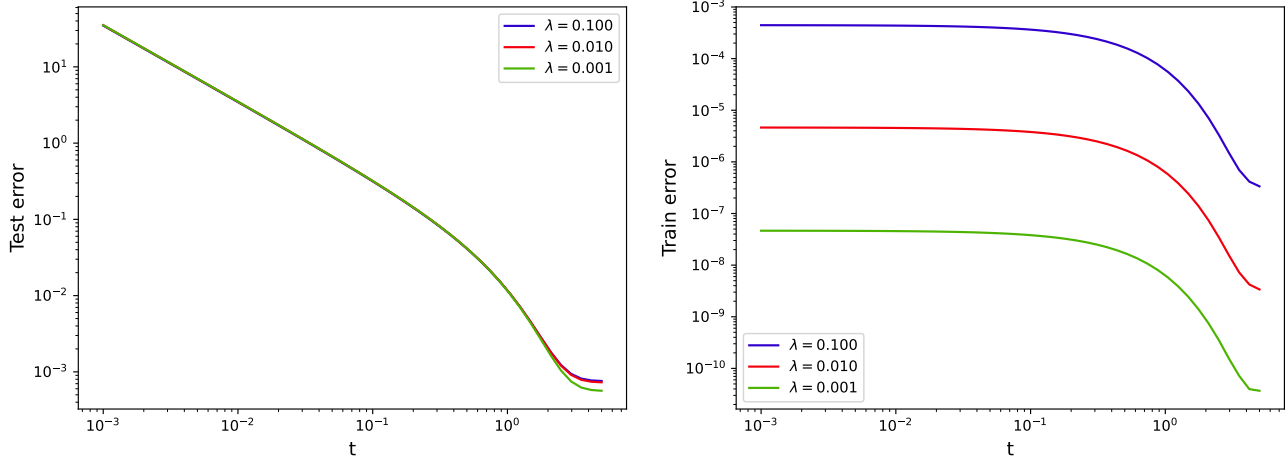


(a) Test and train error as a function of  $t$  for different values of  $\lambda$  for a fixed  $\psi_n = 20.0$  and  $\psi_p = 1024.0$ .

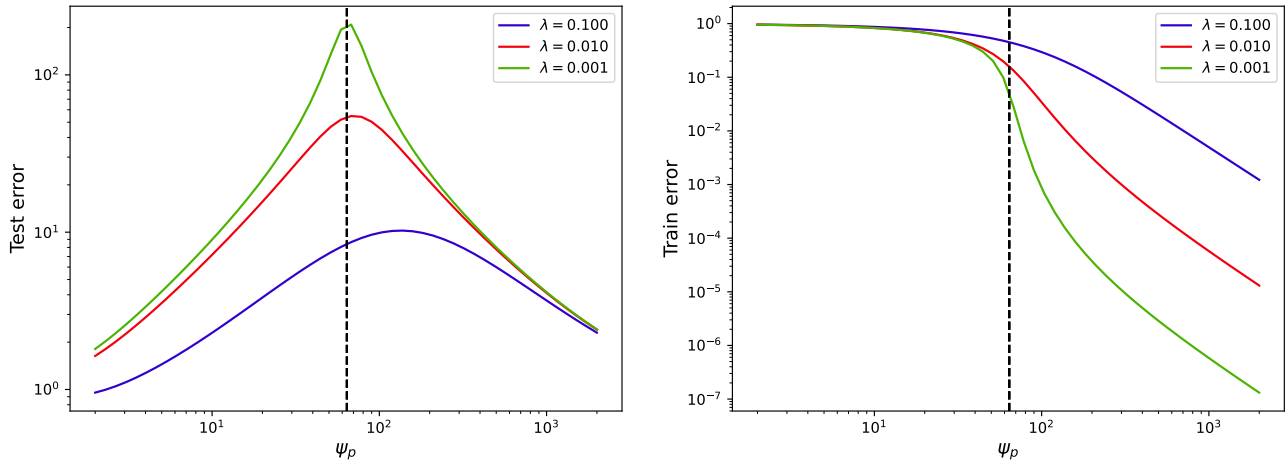


(b) Test and train error as a function of  $\psi_p$  for different values of  $\lambda$  for a fixed  $\psi_n = 64.0$  and  $t = 0.01$ . The dashed vertical line indicates  $\psi_p = \psi_n$ .

Figure 7. Learning curves for different values of  $\lambda$  for  $m = \infty$ . The activation function used is ReLU.



(a) Test and train error as a function of  $t$  for different values of  $\lambda$  for a fixed  $\psi_n = 20.0$  and  $\psi_p = 1024.0$ .



(b) Test and train error as a function of  $\psi_p$  for different values of  $\lambda$  for a fixed  $\psi_n = 64.0$  and  $t = 0.01$ . The dashed vertical line indicates  $\psi_p = \psi_n$ .

Figure 8. Learning curves for different values of  $\lambda$  for  $m = 1$ . The activation function used is ReLU.



Fig. 8 shows the learning errors for  $m = 1$ . In this case, larger values of  $\lambda$  decreases the peak at  $\psi_p = \psi_n$  due to double descent. This is expected since the regularization will help in reducing overfitting.

### D.3. Plots for different activation functions

In this section, we illustrate the behavior of the learning curves for different activation functions: ReLU, tanh, and sigmoid. To make them have the same  $L_2$  norm and  $\mu_0 = 0$ , we introduce proper shiftings and rescalings. Concretely:

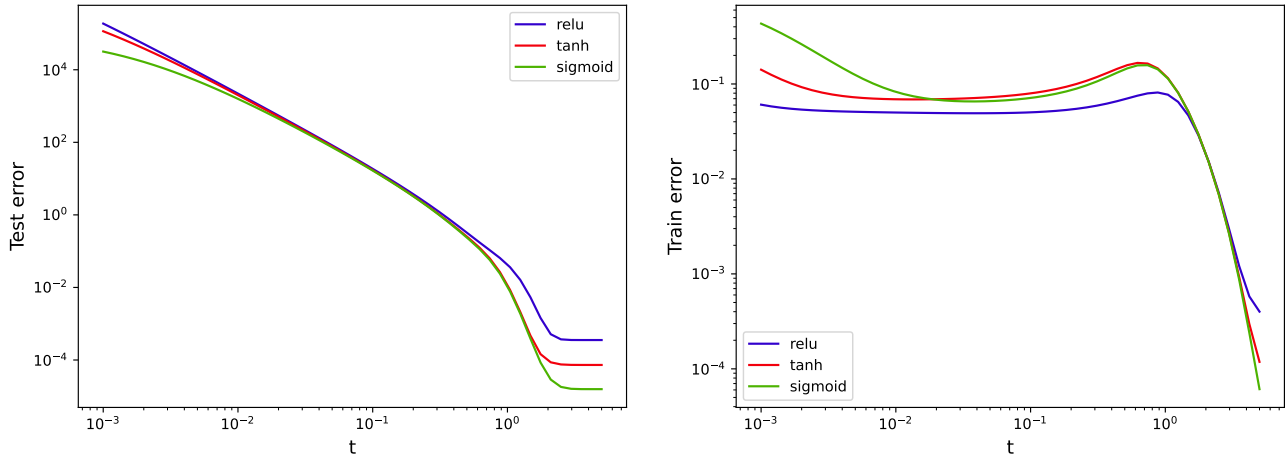
$$\begin{aligned} \text{ReLU}(x) &= x\mathbb{1}\{x \geq 0\} - \frac{1}{\sqrt{2\pi}}, \\ \tanh(x) &= 0.93 \left( \frac{e^x - e^{-x}}{e^x + e^{-x}} \right), \\ \text{sigmoid}(x) &= \frac{2.8}{1 + e^{-x}} - 1.4. \end{aligned}$$

Fig. 9 displays the results for  $m = \infty$ . The activation function enters the analysis through the coefficients  $\mu_1, v, v_0$ , and  $s$ .

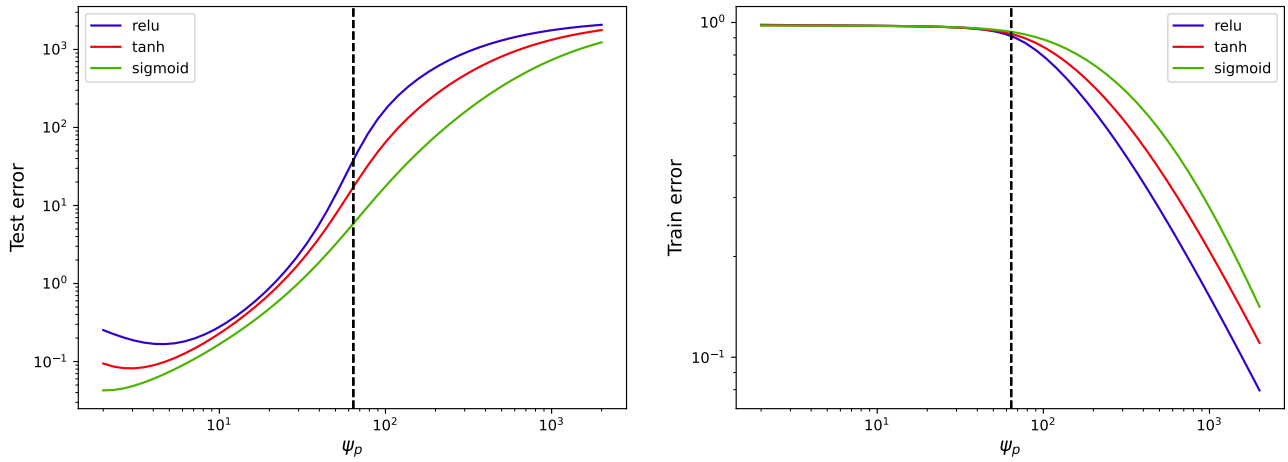
Fig. 10 presents the case  $m = 1$ .

### E. Comparison with Numerically Obtained Learning Curves

Here, we show the learning curves obtained numerically for different values of  $m$ . The test error was illustrated in Fig. 4. In Fig. 11 we exhibit the corresponding train errors as well.

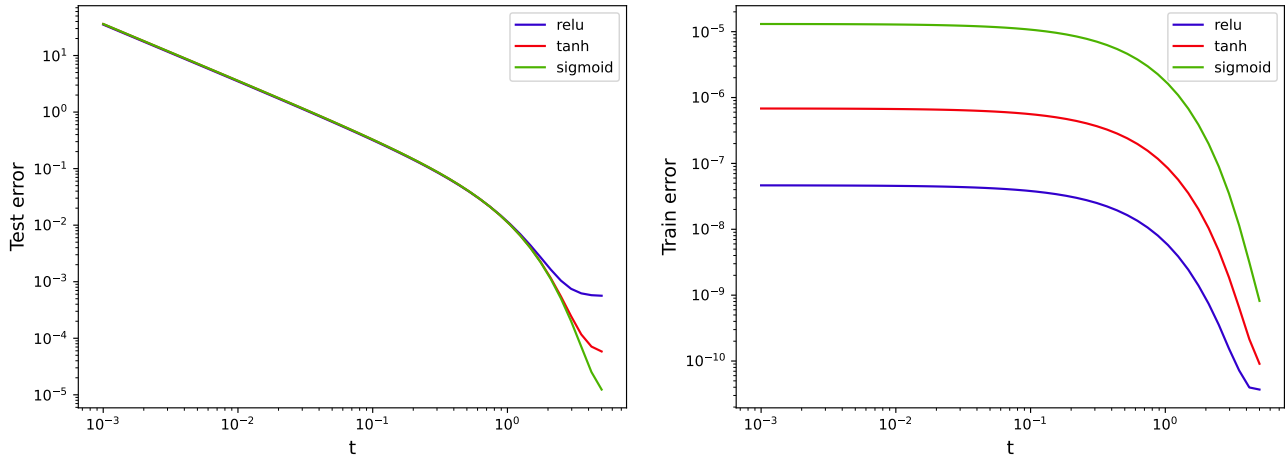


(a) Test and train error as a function of  $t$  for different activation functions for a fixed  $\psi_n = 20.0$  and  $\psi_p = 1024.0$ .

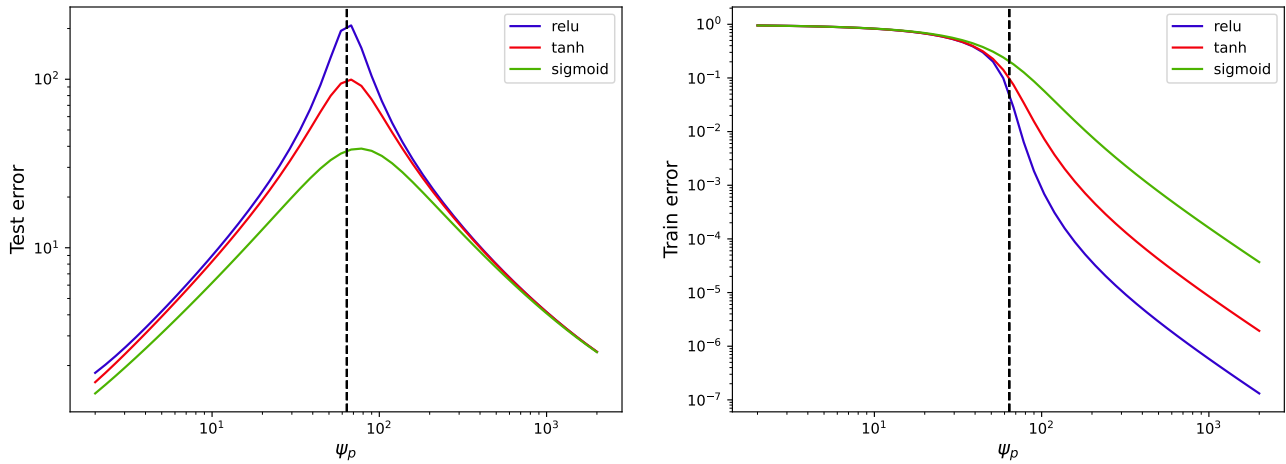


(b) Test and train error as a function of  $\psi_p$  for different activation functions for a fixed  $\psi_n = 64.0$  and  $t = 0.01$ . The dashed vertical line indicates  $\psi_p = \psi_n$ .

Figure 9. Learning curves for different activation functions for  $m = \infty$ . We used  $\lambda = 0.001$ .



(a) Test and train error as a function of  $t$  for different activation functions for a fixed  $\psi_n = 20.0$  and  $\psi_p = 1024.0$ .



(b) Test and train error as a function of  $\psi_p$  for different activation functions for a fixed  $\psi_n = 64.0$  and  $t = 0.01$ . The dashed vertical line indicates  $\psi_p = \psi_n$ .

Figure 10. Learning curves for different activation functions for  $m = 1$ . We used  $\lambda = 0.001$ .

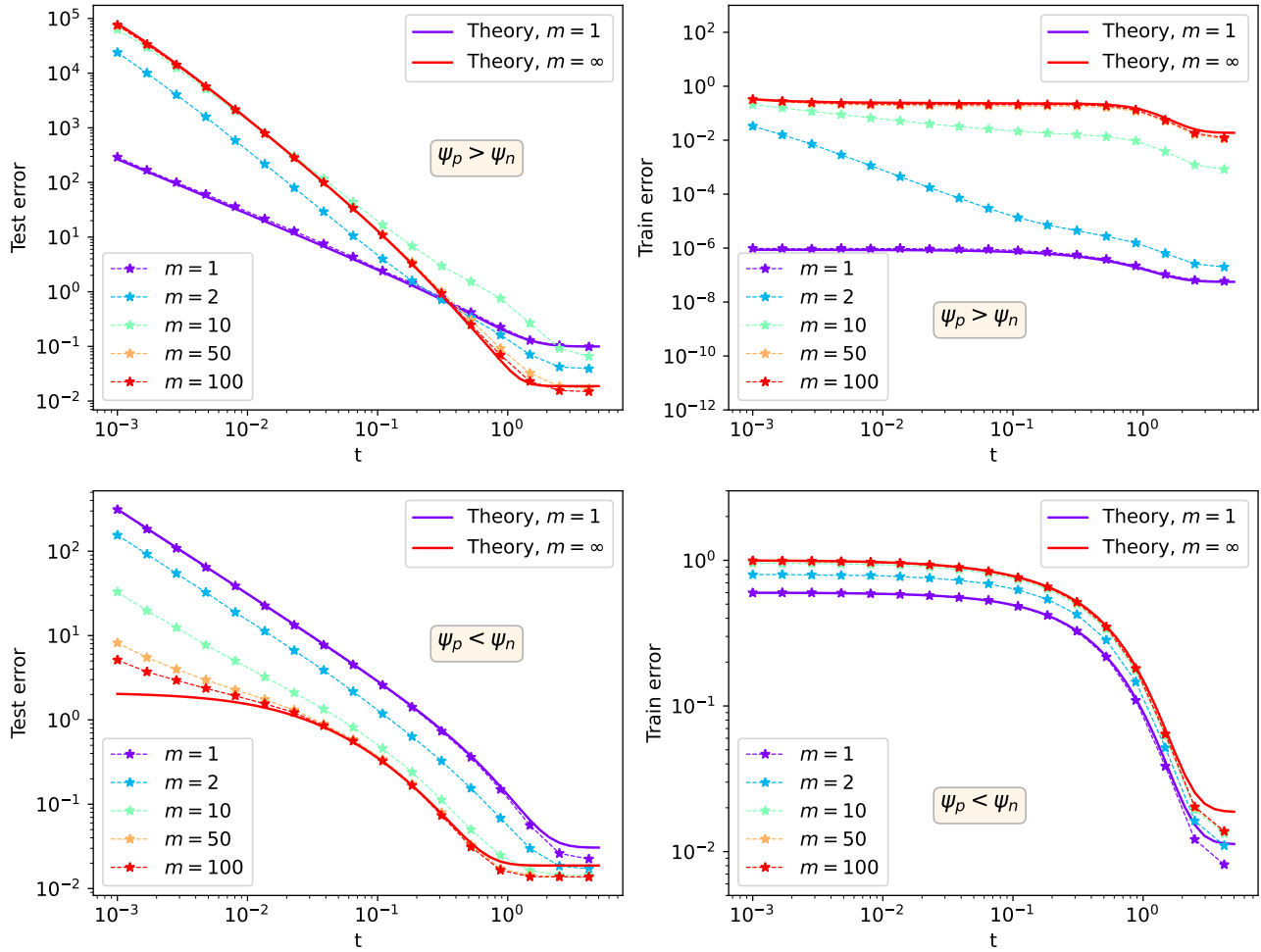


Figure 11. Simulation results ( $d = 100$ ) for different values of  $m$  and fixed  $\psi_p = 20$ ; with  $\psi_n = 2$  (upper plots) and  $\psi_n = 50$  (lower plots). Theoretical results for  $m = 1$  and  $m = \infty$  are depicted as continuous lines.